S duality and framed BPS states via BPS graphs

DONGMIN GANG, PIETRO LONGHI, AND MASAHITO YAMAZAKI

We study a realization of S dualities of four-dimensional $\mathcal{N} = 2$ class $\mathcal{S}$ theories based on BPS graphs. S duality transformations of the UV curve are explicitly expressed as a sequence of topological transitions of the graph, and translated into cluster transformations of the algebra associated to the dual BPS quiver. Our construction applies to generic class $\mathcal{S}$ theories, including those with non-maximal flavor symmetry, generalizing previous results based on higher triangulations. We study the the action of S duality on UV line operators, and show that it matches precisely with the mapping class group, by a careful analysis of framed wall-crossing. We comment on the implications of our results for the computation of three-manifold invariants via cluster partition functions.

1. Introduction and discussion

Twisted compactifications of the six-dimensional $(2,0)$ theory provide a valuable laboratory to explore various nonperturbative aspects of quantum field theories. The archetypal example is perhaps the identification of generalized S-duality for four-dimensional $\mathcal{N} = 2$ dualities with the mapping class groups of Riemann surfaces [1], whose implications have reverberated into the studies of partition functions, BPS line operators, and three-dimensional compactifications, to name a few [2–5].

   In this paper we study S-duality from a low-energy perspective, by going to the Coulomb branch of a four-dimensional class $\mathcal{S}$ theory and asking how dualities act on the BPS spectrum. One advantage of the IR setting is that it gives us a good control on certain observables, allowing us to perform explicit computations. On the other hand, by going the Coulomb branch we apparently lose connection with the UV description of the theory, including the geometric interpretation of S-duality as a mapping class group transformation of the UV curve C. The resolution of this issue comes from studying protected quantities, such as BPS states and their generalizations in presence of line and surface defects, which retain some information about the UV physics. For example, it is known that framed BPS states encode enough information to characterize the algebra of UV line operators [6, 7]. There is in fact a precise map between low-energy line operators and their UV counterparts, developed on spectral networks in [8], where it is called "nonabelianization map". This result provides the conceptual foundation for our approach, explaining how operations on certain low-energy observables can encode UV dualities.

   We derive a low-energy characterization of the mapping class group $\mathrm{MCG}(C)$ of C based on *BPS graphs*, which are graphs embedded in C. BPS graphs arise from a degenerate limit of spectral networks at points in the Coulomb branch where the phases of central charges are maximally aligned, and they encode both the BPS quiver and all the BPS spectra of a theory [9, 10]. There is a whole equivalence class of BPS graphs associated to a given theory, generated by three basic moves shown in Figure 1. The topology of a BPS graph $\mathcal{G}$ is characterized by the type of each vertex (see Figure 1), by the adjacency matrix of its edges, and by a cyclic ordering of edges at each vertex. We identify a mapping class group transformation of C with a sequence of elementary moves κ which takes $\mathcal{G}$ to a new graph $\mathcal{G}'$ with the same topology. In general $\mathcal{G}$ and $\mathcal{G}'$ need not wrap C in the same way, instead they will wrap the UV curve in ways related by an element

$g_\kappa \in \mathrm{MCG}(C)$. There is a natural map $\kappa \to g_\kappa$, that arises from using the BPS graph to characterize the action of κ on $H_1(C, \mathbb{Z})$.
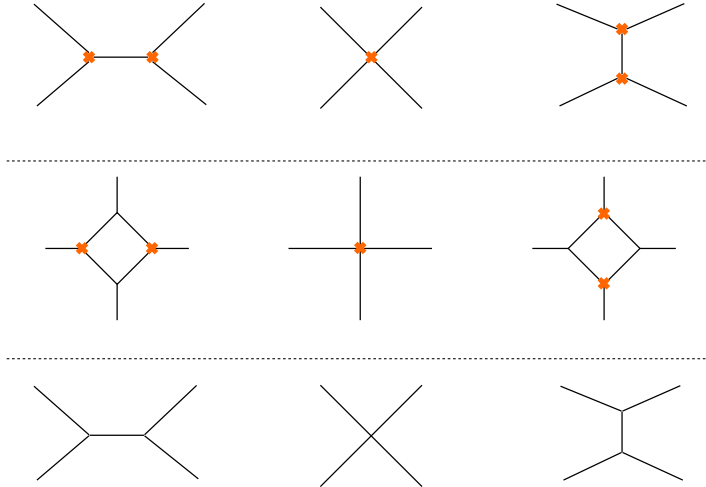

Figure 1: The *flip* move is shown on top, the *cootie* move in the center, and the *j-move* at the bottom. Vertices of BPS graphs come in two types: *branch points* are marked by a yellow cross, *joints* are unmarked.

Our construction of $\mathrm{MCG}(C)$ moreover has a natural interpretation in the context of cluster algebras, because any BPS graph $\mathcal{G}$ is dual to a BPS quiver Q [9]—any sequence κ translates naturally into a sequence of "quiver mutations" of the quiver Q, and into associated sequential changes of cluster variables. The existence of a relation between mapping class groups and cluster algebras has been known for some time [11, 12], however its explicit characterization was limited to Riemann surfaces decorated by "full" punctures, *i.e.* punctures encoding maximal flavor symmetry. Our construction via BPS graphs agrees with these previous results, but further extends to Riemann surfaces with more general types of punctures. The only fundamental requirement for our construction is the existence of a BPS graph for the theory.

The sequence of moves κ that generates a mapping class group transformation can be interpreted as a path in the moduli space of BPS graphs, along which some edges shrink to a point and subsequently grow again. However, finding such a region in the physical moduli space of a theory, which may include both Coulomb and UV parameters, can be challenging. This is

both one of the main shortcomings and advantages of BPS graphs. On the one hand, it is difficult to find the region of moduli space where a BPS graph arises from spectral networks. On the other hand, the BPS graph of a theory is typically so much simpler than the generic network. Based on the experience gained from some examples, we can then make educated guesses for the BPS graphs of more complicated ones. In this paper we follow this approach, and construct the BPS graphs of A_{N-1} theories of class $\mathcal{S}$ defined by a torus with a "simple" puncture using an ansatz inspired by methods of [9]. We thus obtain candidates for the BPS quivers of the so-called $SU(N)$ $\mathcal{N} = 2^*$ theories, and check that the map from $\mathrm{MCG}(C)$ to the cluster algebra is a homomorphism.

A key property of our map from $\mathrm{MCG}(C)$ to cluster algebras is that it reproduces the action of S duality on UV line operators [3, 13–15]. The duality relating BPS graphs to quivers leads to an identification between VEVs of IR line operators and cluster coordinates.[1] Through this relation κ translates into a transformation of the IR line operators of the theory, which can be further mapped into an action on the UV line operators, thanks to a relation between the two sets of observables characterized by framed BPS states [6]. Since a honest BPS graph originates from a spectral network $\overline{\mathcal{G}}$, we can always use the latter to compute the spectrum of framed BPS states, via the nonabelianization map [8]. In this paper we focus on UV line operators $L_\wp$ labeled by closed paths $\wp \subset C$, whose VEVs are identified with traces of holonomies of a flat connection on C. A detailed analysis shows that acting with κ on the underlying spectral network $\overline{\mathcal{G}}$ induces a sequence of framed wall-crossing phenomena. These jumps of framed BPS states translate into a transformation $L_\wp \to L_{g_\kappa(\wp)}$, that maps a UV line operator wrapping $\wp$ into a new one wrapping $g_\kappa(\wp)$. We give a general derivation of this property, which provides a strong check that our construction of S duality via cluster algebras acts in the expected way on UV line operators. We also provide explicit checks of this property for two simple cases: the A_1 theories defined by a once-punctured torus and the four-punctured sphere, as a byproduct we illustrate for the first time computations of VEVs of UV line operators (and framed BPS states) using BPS graphs.[2]

---

[1]More precisely, there is a relation between the two, but they are not quite identical. For example, they have different transformation properties as we explain in the main body of the paper.

[2]More precisely, the computation always relies on the data of the underlying spectral network, and we recover previous results obtained by different, but related, techniques. The point is that it is often easier to work with the BPS graph than

The main novelty of the relation between S duality and cluster algebras uncovered in this paper is the fact that it extends to Riemann surfaces with generic types of punctures. This generalizes previous relations based on (higher) ideal triangulations [11], and relies only on the existence of the BPS graph.

One reason why such a generalization is interesting comes from applications to the study of three-manifold invariants computed by cluster partition functions [16, 17]. A Riemann surface C together with an element κ of its mapping class group define a three-manifold known as a mapping torus $M = C \times_\kappa S^1$. Under suitable conditions on κ, M is a link complement in S^3. The 3d–3d correspondence [4, 5, 18–21] associates a 3d $\mathcal{N} = 2$ theory $T[M]$ to a three-manifold, and in the case when M is a mapping torus, there is a natural quiver Q associated with the theory $T[M]$. Q coincides in fact with the BPS quiver of the 4d $\mathcal{N} = 2$ class $\mathcal{S}$ theory defined by the Riemann surface C, which is dual to the BPS graph. The cluster partition function is a versatile computational tool for studying $SL(N)$ Chern-Simons partition functions on M, whose definition relies precisely on the cluster algebra representation of $\mathrm{MCG}(C)$.

The results of this paper provide the necessary ingredients to compute cluster partition functions for mapping tori fibered by Riemann surfaces with non-maximal punctures. From the viewpoint of Chern-Simons theory, the types of punctures on C enter the definition of the path integral, as they specify the conjugacy class for the holonomy around a cycle along the link (*e.g.* the longitudinal cycle), therefore they characterize the types of topological invariants encoded by the partition function. In particular, for the Chern-Simons path integral on a knot complement with non-generic holonomy along the knot, it is important to sum over saddle points that include several conjugacy classes of holonomies with fixed eigenvalues [22]. Very little is known about these invariants in the case of non-maximal punctures, therefore it will be very interesting to construct them using the cluster algebra realization of mapping class groups developed in this paper; this is the subject of our upcoming work [23]. For the case of a torus with a simple puncture $[N - 1, 1]$ and an element φ of the mapping class group $SL(2, \mathbb{Z})$ (see Section 4.3), the resulting cluster partition function can also be compared with the partition function of $\mathrm{Tr}(T[SU(N), \varphi])$—this is a theory obtained

---

producing the generic spectral network, this can make computations more accessible depending on the context.

by gauging the diagonal $SU(N)$ subgroup of the duality domain wall non-Abelian gauge theory $T[SU(N), \varphi]$, studied in [4]. Schematically, we have

$$(1) \qquad Z_{\mathrm{Tr}(\varphi)}^{\text{cluster partition function}} = Z_{\mathrm{Tr}(T[SU(N),\varphi])}^{\text{3d } \mathcal{N} = 2 \text{ theory}}$$

and this will provide one of the most stringent checks of the BPS graphs and their S duality action proposed in this paper [23].

This paper is organized as follows. Section 2 contains the characterization of S-duality groups (*i.e.* mapping class groups) based on BPS graphs, and the map to cluster algebras. In Section 3 we analyze the framed wall-crossing that is induced by the action of the mapping class group, and show that it reproduces the expected action of S duality on UV line operators. Section 4 contains examples of our construction together with various checks.

2. Mapping class group from BPS graphs

The aim of this section is to explain how a representation of the mapping class group of a Riemann surface can be derived using BPS graphs.

2.1. BPS graphs

A BPS graph $\mathcal{G}$ is a graph embedded in the UV curve C of a class $\mathcal{S}$ theory, and arises as a maximally degenerate spectral network [9] (see also the related works [10, 24, 25]). The shape of the spectral network reflects the geometry of the Seiberg-Witten curve Σ, which is presented as a N-sheeted ramified covering of C, and depends on a choice of Coulomb vacuum and UV moduli. $\mathcal{G}$ appears at a special locus within the moduli space, a.k.a. the *Roman locus*, where central charges of BPS particles all have the same phase ϑ_c (anti-particles have phase $\vartheta_c + \pi$). An important feature of BPS graphs is that they are quite simple, compared to the generic spectral network of a theory. In fact, it is sometimes possible to deduce or guess the BPS graph of a theory without plotting the actual spectral network.[3] In this paper we will mostly take this route, *i.e.* we will adopt an ansatz for the BPS graph of a theory, and will assume that it arises from a honest spectral network at some point of the moduli space. The validity of this assumption is crucial for some of our considerations, and our ansatze for BPS graphs will be supported by several types of checks.

---

[3]This option is important because it can be in practice challenging to find the Roman locus within the moduli space.
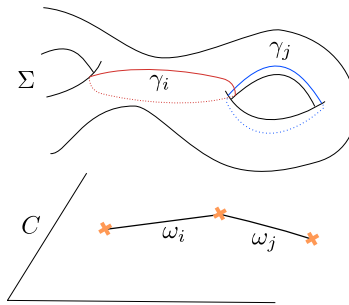
Figure 2: Two elementary webs ω_i, ω_j made of a single edge each, and their lifts to closed cycles on Σ (γ_i and γ_j).

For our purposes, a BPS graph consists of edges $e_i \in E(\mathcal{G})$ attached together at vertices $v \in V(\mathcal{G})$, which come in two types: *branch points* or *joints*. The topological data defining $\mathcal{G}$ includes an embedding in C up to homotopy, the adjacency matrix of its edges, and a cyclic ordering σ_v of edges at each vertex v. $\mathcal{G}$ is naturally divided into smaller connected sets of edges, called *elementary webs*, defined as the connected components of $\mathcal{G}$ after cutting the graph at the branch points (indicated by crosses in figures).[4] An elementary web ω may consist of a single edge, or of several edges connected together at joints. A BPS graph comes equipped with a map from the set of elementary webs to homology cycles on Σ

$$(2) \qquad\qquad h : \omega \mapsto \gamma \in H_1(\Sigma, \mathbb{Z}).$$

This map is inherited from the spectral network: γ is the class of a cycle arising as a lift of ω from C to Σ, see Figure 2. The cyclic ordering σ_v of the edges at each vertex v encodes the intersection pairing $\langle \gamma, \gamma' \rangle$ of cycles associated to webs ω, ω' that meet at v.

Two BPS graphs with the same topological data are regarded as the same graph $\mathcal{G}$. On the other hand, if the embeddings of $\mathcal{G}, \mathcal{G}'$ in C are not homotopy equivalent, we say that $\mathcal{G} \simeq \mathcal{G}'$ are equivalent *as abstract graphs* if there is a 1-1 map f which takes $V(\mathcal{G}) \to V(\mathcal{G}')$ and $E(\mathcal{G}) \to E(\mathcal{G}')$ and

---

[4]This definition of elementary webs is not entirely accurate, but will be appropriate for the BPS graphs studied in this paper. For more details see [9].

respects σ_v at each vertex v

$$(3) \qquad\qquad f(\sigma_v) = \sigma_{f(v)}.$$

This equivalence relation implies that $\mathcal{G}, \mathcal{G}'$ have the same adjacency matrix and same cyclic ordering of edges at each vertex, regardless of how $\mathcal{G}$ and $\mathcal{G}'$ are placed on C. An example of equivalent graphs with different embeddings is shown in Figure 3.

Figure 3: Two BPS graphs on the punctured torus, wrapping it in two different ways related by a mapping class group transformation (a Dehn twist).

2.2. Mapping class group

BPS graphs come in families generated by topological transitions: the *flip*, *cootie* and the *j-move* shown in Figure 1. We will be interested in pairs of equivalent graphs $(\mathcal{G}, \mathcal{G}')$, both embedded in the same Riemann surface C, that are related by a sequence of flips, cooties and j-moves. Let κ_s be a sequence of such moves, which takes $\mathcal{G}$ to an equivalent graph $\mathcal{G}'$, up to a relabeling of the edges κ_r

$$(4) \qquad\qquad \mathcal{G}' \equiv \kappa_r \circ \kappa_s \left(\mathcal{G} \right) \quad \simeq \quad \mathcal{G}.$$

We define κ_r as the relabeling $e_i \to e'_{i'}$ such that $f(e_i) = e'_{i'}$, thereby fixing f in terms of $\kappa_r \circ \kappa_s$ for the rest of the paper. $\mathcal{G}'$ may wrap C in a different way from $\mathcal{G}$, and through the map f relating them we can define a mapping class group transformation for C, under certain conditions which we now specify.

Choose a basis for $H_1(C, \mathbb{Z})$, together with a representative of each basis element made of an oriented closed chain of edges $(e_{i_1}, \ldots, e_{i_k})$ of $\mathcal{G}$. The map f takes this to a new chain $(e'_{i_1}, \ldots, e'_{i_k}) \subset E(\mathcal{G}')$ which is also closed, since $\mathcal{G} \simeq \mathcal{G}'$. The new chain defines a new element of $H_1(C, \mathbb{Z})$. In order

to define a honest mapping class group transformation, we require that any two chains of edges in $E(\mathcal{G})$ in the same homology class

$$(5) \qquad\qquad [(e_{i_1}, \ldots, e_{i_k})] = [(e_{j_1}, \ldots, e_{j_\ell})]$$

must be mapped to two chains in $E(\mathcal{G}')$ which are also in the same homology class.

$$(6) \qquad\qquad \left[(e'_{i_1}, \ldots, e'_{i_k})\right] = \left[(e'_{j_1}, \ldots, e'_{j_\ell})\right] \ .$$

If this condition is satisfied, f acts as an endomorphism of $H_1(C, \mathbb{Z})$, and can be identified with a mapping class group transformation. We will henceforth restrict our attention to sequences κ_s composed with relabelings κ_r which lead to equivalent graphs $\mathcal{G}, \mathcal{G}'$ related by a map f satisfying this requirement. Since we fixed f in terms of $\kappa_r \circ \kappa_s$ we will leave f implicit in the following, and simply refer to the operation $\kappa = \kappa_r \circ \kappa_s$ as a mapping class group transformation.
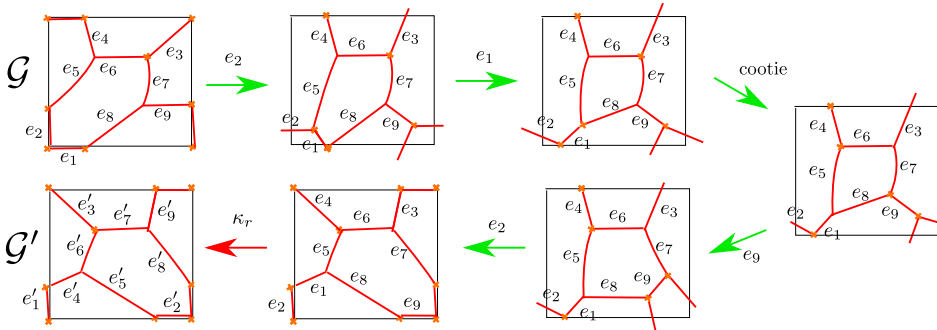

Figure 4: The BPS graph $\mathcal{G}$ is placed on a torus with one puncture, whose fundamental domain is depicted as a square, with the puncture placed at the corners. $\mathcal{G}$ undergoes a sequence of moves κ_s (green arrows) followed by the relabeling κ_r.

This construction can be made quite explicit: given κ satisfying the consistency conditions, it can be identified with a specific element g_κ of the mapping class group. For example let us consider the sequence of moves on the BPS graph shown in Figure 4. κ_s consists of the following moves: flip e_2, flip e_1, cootie on (e_5, e_6, e_7, e_8), flip e_9, flip e_2. The graph obtained after applying κ_s has a $\mathbb{Z}_3$ symmetry, so there are three inequivalent relabelings

$\kappa_r, \kappa_r', \kappa_r''$ that can be used to produce a new BPS graph $\mathcal{G}'$ equivalent to the original one. We choose κ_r as

$$(7) \qquad \kappa_r : \begin{cases} e_2 \to e_1 \to e_4 \to e_3 \to e_9 \to e_2 \\ e_5 \to e_6 \to e_7 \to e_8 \to e_5, \end{cases}$$

meaning that $\kappa_r(e_2) = e_1'$, et cetera. Next we choose generators for $H_1(C, \mathbb{Z})$ as the homology classes of the following sequences of edges of $\mathcal{G}$

$$(8) \qquad A : [(e_1, e_8, e_9, e_2)], \qquad B : [(e_2, e_5, e_4, e_1)].$$

The orientation of a cycle is understood as *left to right*, when reading each sequence. As the moves κ_s are applied to $\mathcal{G}$, we keep track of these edges, and finally apply the relabeling κ_r. This leads to a new pair of cycles, defined by the new sequences of edges identified by the equivalence $\mathcal{G} \simeq \mathcal{G}'$

$$(9) \qquad A' : [(e_1', e_8', e_9', e_2')], \qquad B' : [(e_2', e_5', e_4', e_1')].$$

As homology classes, they are related to the original ones by

$$(10) \qquad A' = B, \qquad B' = -A,$$

therefore we identify κ with the following generator of $\text{MCG}(C) \simeq SL(2, \mathbb{Z})$

$$(11) \qquad g_\kappa = S^{-1} = \begin{pmatrix} 0 & -1 \\ 1 & 0 \end{pmatrix}.$$

More generally, a transformation which takes A, B to $A' = dA + cB$, $B' = bA + aB$ corresponds to the following element of $SL(2, \mathbb{Z})$

$$(12) \qquad g_\kappa = \begin{pmatrix} a & b \\ c & d \end{pmatrix}.$$

This representation of g_κ obviously depends on the choice of homology basis on C, and different choices should be related by conjugation. Therefore upon fixing a basis, any two sequences κ, κ' must satisfy

$$(13) \qquad g_{\kappa'} g_\kappa = g_{\kappa' \circ \kappa}.$$

2.3. Map to cluster algebra

A BPS graph $\mathcal{G}$ is dual to a BPS quiver Q: an oriented graph consisting of nodes Q_0 connected by arrows Q_1 [26, 27]. Nodes are in 1-1 correspondence

with elementary webs of $\mathcal{G}$, we associate to the i-th node the generator $\gamma_i = h(\omega_i)$ of the charge lattice identified by (2). There are $b_{ij} = -\langle \gamma_i, \gamma_j \rangle$ arrows oriented from node i to node j, when counted with signs.[5] Figure 5 shows the BPS quiver dual to the initial BPS graph of Figure 4, node label i stands for γ_i. Since the pairing $\langle \gamma_i, \gamma_j \rangle$ is determined by the adjacency matrix of $\mathcal{G}$ and by the cyclic orderings $\{\sigma_v\}_{v \in V(\mathcal{G})}$, two equivalent graphs $\mathcal{G} \simeq \mathcal{G}'$ are dual to the same BPS quiver.
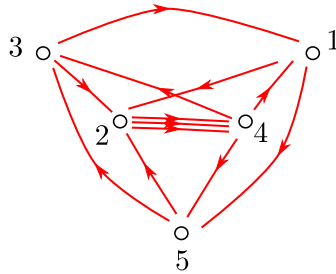

Figure 5: BPS quiver dual to the graphs $\mathcal{G}$ and $\mathcal{G}'$ of Figure 4.

A quiver further encodes the information of an associated cluster algebra [28, 29]. Let y_i be a set of variables associated to each node of Q. The pair $(Q, \{y_i\})$ defines a *seed* for the cluster algebra. The algebra is generated by an elementary operation on the seed, known as a mutation. A mutation μ_k on node k produces a new quiver with the same set of nodes but with new arrows

$$(14) \qquad b'_{ij} = \begin{cases} -b_{ij} & \text{if } i = k \text{ or } j = k, \\ b_{ij} + \frac{1}{2} \left(|b_{ik}| b_{kj} + b_{ik} |b_{kj}| \right) & \text{otherwise.} \end{cases}$$

The mutation also acts on the cluster variables[6] by

$$(15) \qquad y'_i = y_i y_k^{[-b_{ik}]_+} \left(1 + y_k^{-1} \right)^{-b_{ik}},$$

---

[5] Negative values of b_{ij} mean that the arrows go from j to i. This definition assumes that quivers do not contain two-cycles or loops, and is appropriate for the purposes of this paper. A more general dictionary between quivers and BPS graphs can be found in [9].

[6] More precisely cluster y-variables [29]. In this paper a cluster variable always means a cluster y-variable.

where $[a]_+$ is zero if a is negative, and equal to a otherwise. The flip move on a BPS graph corresponds to a mutation on the dual quiver, performed on the node corresponding to the shrinking edge, see Figure 6. The cootie and j-move leave the quiver invariant instead.

Going back to the mapping class group, let us consider the action of a sequence $\kappa : \mathcal{G} \mapsto \mathcal{G}'$ on the quiver. The sequence κ_s translates into a sequence of mutations, while the relabeling κ_r maps to a simultaneous reshuffling of the quiver nodes and cluster variables. Overall, the composite operation $\kappa = \kappa_r \circ \kappa_s$ must take Q back to itself since equivalent BPS graphs have identical quivers. Nevertheless, the resulting transformation on the cluster variables needs not be trivial, and we take it as the definition of the action of κ on the cluster algebra. In this sense, through BPS graphs we have given a representation of the mapping class group of C in the cluster algebra.

The fact that mapping class groups of surfaces admit a cluster algebra representation is not new, in fact such maps have been constructed by several other authors, see for example [11, 12, 30–33]. However, most of the previous constructions are limited to cluster varieties associated to Riemann surfaces decorated by *full* punctures, *i.e.* corresponding to maximal flavor symmetry (exceptions include [17, 34]). We both re-derive these previous constructions via BPS graphs, and extend them to cases including partially higgsed punctures, for which BPS graphs can be defined. In Section 4 we provide several examples of this construction of mapping class groups from cluster algebras, in higher rank theories of class $\mathcal{S}$ defined by Riemann surfaces decorated with simple punctures, *i.e.* with minimal flavor symmetry.
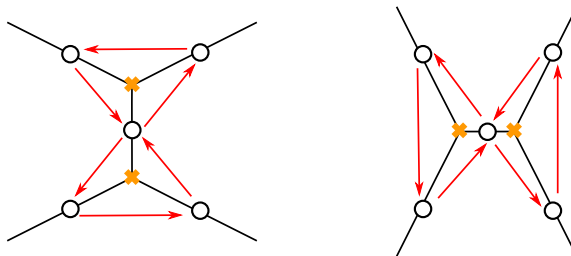

Figure 6: The flip of an edge of the graph and the mutation it induces of the dual BPS quiver.

3. S-duality on framed BPS states

This section is devoted to studying the action of the generalized S-duality group on UV line operators. We will show that our construction of the mapping class group of C based on transitions of BPS graphs is consistent with the action of dualities on a certain class of UV observables. Related questions about the action of cluster algebras on UV line defects were studied in [35, 36] from the viewpoint of framed BPS quivers.[7]

A crucial assumption in our derivation will be that the BPS graph always arises from a degenerate limit of spectral networks. This analysis leads to two consequences. If a BPS graph is known to arise from a degenerate spectral network, it is guaranteed that the representation of MCG(C) from Section 2 acts correctly on a certain class of UV line operators. On the other hand, if $\mathcal{G}$ is a conjectural BPS graph, and the corresponding mapping class group action behaves appropriately (in a sense that will be defined in this section), this provides a strong consistency check that $\mathcal{G}$ actually arises as a degenerate limit of spectral networks, and is therefore the physical BPS graph of the theory.

3.1. Connecting IR and UV line operators

The Hitchin system defined by the class $\mathcal{S}$ data (A_{N-1}, C, D) is a hyper-Kähler manifold, that in complex structure J_ζ (with $\zeta \in \mathbb{C}^*$) can be viewed as a moduli space of flat $GL(N)$ connections over C. There is a standard set of coordinates on this moduli space, namely traces of holonomies along cycles in $H_1(C, \mathbb{Z})$. The traces of these holonomies bear the interpretation of expectation values of a certain class of BPS line operators in the gauge theory [3, 6, 14, 15, 38]. Let $\wp$ be a closed path on C, we will denote the corresponding UV line operator by $L_\wp^{(\mathrm{UV})}$.

On the Coulomb branch $\mathcal{B}$, the gauge symmetry is broken to an Abelian torus $U(1)^r$, and the set of line operators of the IR theory is therefore quite

---

[7]An interesting generalization of the line defects considered in this section, is to consider those described by *laminations* in A_1 theories [6]. Vevs of UV line defects labeled by laminations can be computed with spectral networks, see for example [37], therefore we expect that our construction of the mapping class group can be extended to this setting. Laminations arise in class $\mathcal{S}$ theories defined by a Riemann surface with one or two irregular punctures. The mapping class group is thus $\mathbb{Z}_k$, the discrete rotations of the plane (or cylinder), and the S-duality reduces to a manifestation of the Witten effect on the core charge of the line defects [36]. We thank M. Cirafici for bringing our attention to this point.

different from that of the UV theory. Line operators in the IR are classified by electromagnetic charges γ valued in $H_1(\Sigma, \mathbb{Z})$, where Σ is the spectral curve of the Hitchin system in a fixed vacuum $u \in \mathcal{B}$. We will denote the corresponding line operator by $L_\gamma^{(\mathrm{IR})}$. Just like for UV line operators, the expectation value of $L_\gamma^{(\mathrm{IR})}$ can be interpreted as the holonomy of a $GL(1)$ connection over Σ.

The dictionaries between UV/IR line operators and holonomies can be used to establish a relation between the two sets of observables, based on a relation between the two moduli spaces of flat connections. This goes by the name of *nonabelianization map*, and can be characterized via spectral networks [8]. A spectral network $\mathcal{W}$ on C defines a map

$$(16) \qquad \Psi_\mathcal{W} \; : \; \mathcal{M}_{\mathrm{flat}}(GL(1), \Sigma) \; \longrightarrow \; \mathcal{M}_{\mathrm{flat}}(GL(N), C),$$

that associates to any smooth closed path $\wp$ on C a formal parallel transport $F(\wp; \mathcal{W})$ for the flat $GL(N)$ connection on C. The trace of holonomy can be expanded as follows

$$(17) \qquad \mathrm{Tr} F(\wp; \mathcal{W}) = \sum_\gamma \overline{\Omega}(\mathcal{W}, \gamma, \wp) X_\gamma,$$

where X_γ are formal variables representing $GL(1)$ holonomies along cycles $\gamma \in H_1(\Sigma, \mathbb{Z})$. The coefficients $\overline{\Omega}(\mathcal{W}, \gamma, \wp)$ depend on $\wp$ only through its homotopy class, this highly nontrivial property justifies the interpretation of $F(\wp, \mathcal{W})$ as the parallel transport of a flat $GL(N)$ connection. Physically $\overline{\Omega}(\mathcal{W}, \gamma, \wp)$ is an index which counts *framed BPS states*, semiclassically these can be viewed as supersymmetric boundstates of BPS particles and the line operator [6, 39–43], whereas mathematically they encode the relation between the two sets of holonomies. By the dictionary relating holonomies to VEVs of line operators

$$(18) \qquad \langle L^{(\mathrm{UV})} \rangle \sim \mathrm{Tr} F(\wp, \mathcal{W}), \qquad \langle L^{(\mathrm{IR})} \rangle \sim X_\gamma,$$

the expansion in framed BPS states (17) therefore encodes the relation between the VEVs.

This relation between UV and IR line operators will play a key role towards our goal of studying the action of $\mathrm{MCG}(C)$ on the former. Recall that a BPS graph $\mathcal{G}$ provides a basis for the IR charge lattice through the map (2), at least locally in some patch of the Coulomb branch. On the other hand, $\mathcal{G}$ should first and foremost arise as a degenerate spectral network, and therefore can be used to compute framed BPS states. In the rest of this

section we will explain how to formulate the nonabelianization map (17) entirely in terms of the data associated to a BPS graph. In particular, we propose a relation between the formal variables X_γ and the cluster coordinates y_i [8, 9], and use it to define the action of MCG(C) on UV line operators via nonabelianization.

3.2. Resolved BPS graphs

Let $\mathcal{G}$ be a BPS graph on C arising from a maximally degenerate spectral network $\mathcal{W}(u, \vartheta_c)$ at a point u on the Roman locus, and critical phase ϑ_c.[8] There are two canonical resolutions of $\overline{\mathcal{G}}$, corresponding to positive or negative perturbations of the phase ϑ_c involved in the definition of a network spectral network. These two options are known as the *American* and the *British* resolution [8].[9] Note that resolving the spectral network is a necessary condition for the nonabelianization map (17) to be well-defined. We choose to resolve by going to a phase $\vartheta_c - \epsilon$, known as the *American resolution* of $\mathcal{W}_c$, and denote the resolved network by $\overline{\mathcal{G}}$ to stress its relation to the BPS graph $\mathcal{G}$. In practice, resolving $\mathcal{W}_c \to \overline{\mathcal{G}}$ amounts to replacing the unoriented edges with families of oriented edges running "on the right", as shown in the bottom-left frame of Figure 7. The oriented edges of a spectral network can be sourced either at branch points or at joints, and their precise shape is determined by the geometry of the spectral curve Σ. Since $\overline{\mathcal{G}}$ is the American resolution of a BPS graph, for small ϵ the oriented edges will typically run very close to the original shape of $\mathcal{G}$, although they may eventually veer off and be captured by punctures, after a very long time.

Next let us consider two equivalent BPS graphs $\mathcal{G}, \mathcal{G}'$ related by a sequence $\kappa = \kappa_r \circ \kappa_s$. First of all, it is important to realize that $\mathcal{G}, \mathcal{G}'$ are generally related to two different spectral curves Σ, Σ'. In other words, if we assume that $\mathcal{G}, \mathcal{G}'$ arise from actual spectral networks on C, they would occur in different regions of the moduli space of the theory.[10] Therefore homology classes encoded by the respective elementary webs through the map (2) belong to distinct homology lattices $H_1(\Sigma, \mathbb{Z})$ and $H_1(\Sigma', \mathbb{Z})$. In order to compare charges γ between $\mathcal{G}$ and $\mathcal{G}'$ we must specify a parallel transport

---

[8]Note that the spectral network $\mathcal{W}_c$, which also looks like a graph on C, may contain more edges than $\mathcal{G}$. See for example [9, Fig. 19]. It is important to retain all the edges of the network.

[9]Apologies to the rest of the world.

[10]This would mean different loci on the Coulomb branch, but possibly also different Coulomb branches, related by deformations of UV moduli like masses and couplings.
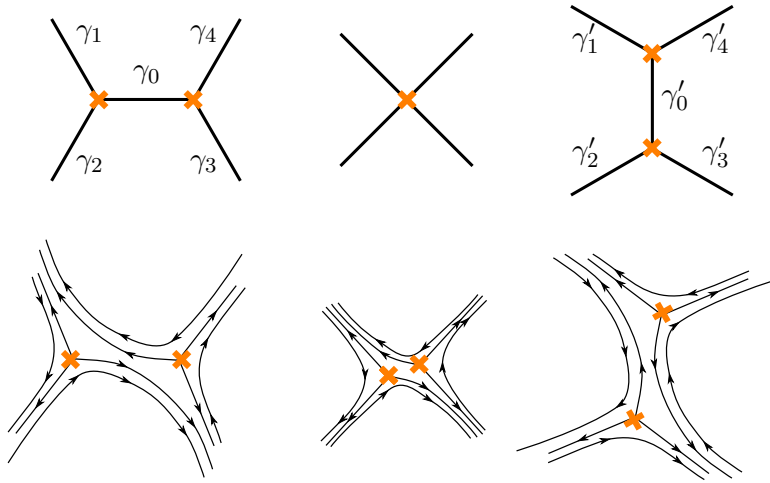
Figure 7: The flip move on a BPS graph $\mathcal{G}$, and the corresponding deformation of the spectral network corresponding to the American resolution of $\mathcal{G}$. The resulting spectral network *does not* coincide with the American resolution of the BPS graph after the flip.

for the homology lattice, through the sequence of transitions κ that takes $\mathcal{G}$ to $\mathcal{G}'$. Happily, there is a canonical way to do this suggested by our choice of a resolution, which allows to smoothly deform homology classes throughout κ. In physical terms, working with resolved spectral networks $\overline{\mathcal{G}}$ instead of the actual BPS graph, we always avoid singularities of the moduli space where branch points collide. At these singularities a cycle of Σ shrinks, and the Picard-Lefshetz monodromy of the charge lattice would introduce an ambiguity. Instead of colliding branch points, we deform the network in a way that they "scatter off" each other, as shown in Figure 7. In keeping with the choice of American resolution, we will adopt the convention that after the scattering each branch point veers off to its right. Overall the sequence of moves κ_s, together with this convention on the motion of branch points through flips, unambiguously fixes a parallel transport for $H_1(\Sigma, \mathbb{Z})$. We stress that using this parallel transport is crucial for making sense of any relation between homology cycles γ_i and γ_i' associated respectively to elementary webs of $\mathcal{G}$ and $\mathcal{G}'$. This identification of charges by parallel transport in the moduli space will henceforth be understood for the rest of the discussion.

Having settled the question of comparing homology lattices of different spectral curves, there is one additional subtlety to confront, in order to relate the charges γ_i to γ_i' associated to elementary webs of $\mathcal{G}$ and $\mathcal{G}'$. This is the fact that the map (2) which associates homology classes to edges of $\mathcal{G}$ actually *jumps* in correspondence of a flip. This jump is clearly necessary, because a flip on $\mathcal{G}$ acts by a mutation on the dual quiver Q, and its arrows correspond to the intersection pairing $b_{ij} = \langle \gamma_j, \gamma_i \rangle$ of the charges assigned by h to elementary webs. Referring to Figure 7 the jump of h reads[11]

$$\begin{gathered} \gamma_0' = -\gamma_0, \quad \gamma_1' = \gamma_1 + \langle \gamma_1, \gamma_0 \rangle \gamma_0, \quad \gamma_2' = \gamma_2, \\ \gamma_3' = \gamma_3 + \langle \gamma_3, \gamma_0 \rangle \gamma_0, \quad \gamma_4' = \gamma_4, \end{gathered}$$
(19)

in agreement with (14).[12]

A mutation of the quiver induces a cluster transformation (15) on the cluster variables y_i. Therefore cluster variables y_i, y_i' of quivers Q, Q' dual to $\mathcal{G}, \mathcal{G}'$ must be related by a sequence of cluster mutations, possibly composed with a permutation, corresponding respectively to the flips in κ_s and to relabelings in κ_r. By a slight abuse of notation we will denote this relation by
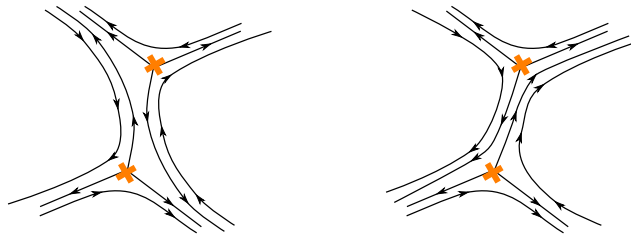
$$y_i' = \kappa(y_i).$$
(20)

Figure 8: An inverse $\mathcal{K}$-wall transition of a spectral network.

The jump of h may appear in contradiction with the continuity of the transport of the charge lattice described previously, instead there is a rather

---

[11] This is one place where the choice of American resolution is relevant. In British resolution we should employ a different transformation.

[12] The transformation (19) coincides with the transformation properties of (the logarithm of) the so-called tropical y-variables in the cluster algebras.

subtle interplay between the two. The parallel transport of the homology lattice is defined by choosing a resolution $\overline{\mathcal{G}}$ of the initial BPS graph $\mathcal{G}$. However a flip transition on $\overline{\mathcal{G}}$ will *not* produce a network that is a resolution of the new BPS graph, as made evident in Figure 7. In this example the new spectral network in the bottom-right frame differs from the American resolution of the BPS graph in the top-right frame, since the two vertical oriented edges in the middle run "on the left". In fact, there is a precise relation between this spectral network and the resolution of the new BPS graph, which is known as a $\mathcal{K}$-*wall transformation* and shown in Figure 8. This is a jumps of the spectral network which involves a change of its topology, and induces a transformation of both the $\overline{\Omega}$ and the X_γ appearing in (17) [8].

In conclusion, we *define* the parallel transport of the homology lattice by moving branch points through a flip transition, as shown in Figure 7. Note that the deformation of the spectral curve, as reflected by the motion of branch points over C, does not imply any choice about what we do with the spectral network. On the other hand this deformation produces non-canonical spectral networks, in the sense that the resulting network doesn't correspond to the resolution of a BPS graph, but is related to one precisely by $\mathcal{K}$-wall transitions. We therefore perform a $\mathcal{K}$-wall transformation on the network $\overline{\mathcal{G}}$, to compensate for this mismatch. At the same time, we also introduce a jump (19) for the map h which associates homology cycles γ_i to elementary webs of $\mathcal{G}$. This change of basis for the charge lattice will be denoted by

$$(21) \qquad\qquad \gamma_i' = \kappa(\gamma_i)$$

by a small abuse of notation. It is understood that $\kappa = \kappa_r \circ \kappa_s$ also includes the effect of the relabeling κ_r, which acts by a permutation on the basis.

3.3. Nonabelianization for BPS graphs

Let us recall some key properties of the computation of framed BPS indices $\overline{\Omega}(\overline{\mathcal{G}}, \gamma, \wp)$ using spectral networks. The $\overline{\Omega}$ are entirely determined by how the path $\wp$ intersects the spectral network $\overline{\mathcal{G}}$, and by the topology of the network. The contribution of each intersection is determined by a combinatorial problem formulated in terms of the overall topology of $\overline{\mathcal{G}}$. When the network arises as the resolution of a BPS graph, the combinatorial data, a.k.a. 2d-4d soliton data, can be computed directly in terms of topological data of $\overline{\mathcal{G}}$ which includes a cyclic ordering of edges at each vertex [10]. A bit

more precisely, the construction of $F(\wp, \overline{\mathcal{G}})$ depends on which oriented edges are crossed by $\wp$, but the final result is actually invariant under homotopy of the latter, including deformations across branch points and joints of $\overline{\mathcal{G}}$.

Through the map (2) the elementary webs provide a basis $\gamma_i \in H_1(\Sigma, \mathbb{Z})$ for the IR charge lattice. Any charge γ therefore admits a unique decomposition $\gamma = \sum_i c_i \gamma_i$ and can be represented by a lattice vector $\mathbf{c} = (c_1, \ldots, c_d)$,[13] where d is the number of elementary webs of $\mathcal{G}$ and coincides with the rank of the charge lattice. We can therefore reformulate the nonabelianization map entirely in terms of data of $\overline{\mathcal{G}}$ as follows

$$(22) \qquad \operatorname{Tr} F(\wp; \overline{\mathcal{G}}) = \sum_{\mathbf{c}} \overline{\underline{\Omega}}(\overline{\mathcal{G}}, \mathbf{c}, \wp) X_{\mathbf{c}}$$

without any explicit reference to $H_1(\Sigma, \mathbb{Z})$. It is always possible to bring this expression back to the form (17), through the map (2). This expression of holonomies is especially convenient for studying the action of $\mathrm{MCG}(C)$ derived in Section 2, we turn to this next.

3.4. Mapping class group action on holonomies

Consider two equivalent BPS graphs $\mathcal{G}$ and $\mathcal{G}'$ related by a sequence κ, we would like to study how the respective holonomies (22) are related. Recall that to compute these holonomies one should work with non-degenerate spectral networks, and we will choose $\overline{\mathcal{G}}, \overline{\mathcal{G}}'$ as defined previously.[14] The computation of $\overline{\underline{\Omega}}$ depends on two pieces of information: how $\wp$ intersects $\overline{\mathcal{G}}$, and certain combinatorial data computed from $\overline{\mathcal{G}}$. The latter is known as *soliton data*, and is entirely determined by the topology of the spectral network. By definition $\mathcal{G}$ and $\mathcal{G}'$ have the same topology, just different embeddings in C, and the same will be assumed of $\overline{\mathcal{G}}$ and $\overline{\mathcal{G}}'$. This implies that the soliton data of $\overline{\mathcal{G}}$ and $\overline{\mathcal{G}}'$ must be essentially identical, the only difference between the two will be in the map h, which plays the role of translating combinatorial data on a BPS graph into homology classes on Σ.

A bit more precisely, the soliton data of $\overline{\mathcal{G}}$ consists of relative homology classes, counting paths on Σ which run "above" edges of $\overline{\mathcal{G}}$ according to the projection $\pi : \Sigma \to C$ [8]. This data is determined by a set of equations,

---

[13]This is known as the *c*-vector in cluster algebras [29].

[14]It is important to distinguish from the situation of Figure 7. Here we always take the *actual* American resolution both for $\mathcal{G}$ and for $\mathcal{G}'$. As explained previously, we perform $\mathcal{K}$-wall transitions on the network at each flip, in order to preserve this property.

which can be formulated entirely in terms of the adjacency matrix of $\overline{\mathcal{G}}$ and of the cyclic ordering of edges at its vertices [10]. Therefore the equations that determine soliton data are formally identical for $\overline{\mathcal{G}}$ and for $\overline{\mathcal{G}}'$, and there is a 1-1 correspondence between them. However the spectral networks $\overline{\mathcal{G}}, \overline{\mathcal{G}}'$ encode different framed BPS states. This is because the respective elementary webs of $\mathcal{G}$ and $\mathcal{G}'$ define different bases of the IR charge lattice, related by jumps of the map (2).

The fact that soliton data sets are formally identical implies that the integers

$$(23) \qquad \underline{\overline{\Omega}}(\overline{\mathcal{G}}, \mathbf{c}, \wp) = \underline{\overline{\Omega}}(\overline{\mathcal{G}}', \mathbf{c}', \wp')$$

coincide if

$$(24) \qquad \mathcal{G}' = \kappa(\mathcal{G}), \quad \mathbf{c}' = \mathbf{c}, \quad \wp' \simeq g_\kappa(\wp),$$

as a direct consequence of the construction of (22). The first requirement states that $\mathcal{G} \simeq \mathcal{G}'$ must be equivalent as abstract graphs, and are moreover related by a sequence of moves $\kappa = \kappa_r \circ \kappa_s$. The second relation is simply an identity of vectors in $\mathbb{Z}^n$. The third relation denotes equivalence as homology classes $[\wp]$ and $[\wp']$, related by the mapping class group transformation g_κ associated to κ.

Combining the identity (23) with the change of basis for the charge lattice (21) we arrive the following formula, which relates the holonomy computed along $\wp$ using $\overline{\mathcal{G}}'$ to the one along $\wp$ computed using $\mathcal{G}$

$$
\begin{aligned}
(25) \qquad \mathrm{Tr} F(\wp'; \overline{\mathcal{G}}') &= \sum_{\mathbf{c}'} \underline{\overline{\Omega}}(\overline{\mathcal{G}}', \mathbf{c}', \wp') X_{c_i' \gamma_i'} \\
&= \sum_{\mathbf{c}} \underline{\overline{\Omega}}(\overline{\mathcal{G}}, \mathbf{c}, \wp) X_{c_i \gamma_i'} \\
&= \sum_{\mathbf{c}} \underline{\overline{\Omega}}(\overline{\mathcal{G}}, \mathbf{c}, \wp) X_{c_i \kappa(\gamma_i)}.
\end{aligned}
$$

We can also ask how does the holonomy around a fixed path $\wp'$ change, as the network undergoes a sequence of flips and cooties κ_s. Recall that we smoothly deform the spectral network from $\overline{\mathcal{G}}$ to $\overline{\mathcal{G}}'$, except for a $\mathcal{K}$-wall jump at each flip, therefore

$$(26) \qquad \mathrm{Tr} F(\wp', \overline{\mathcal{G}}') = \mathcal{K}_n^{-1} \cdots \mathcal{K}_1^{-1} \left(\mathrm{Tr} F(\wp', \overline{\mathcal{G}}) \right),$$

provided that the homology cycles γ appearing in the expansion of either side are identified according to the parallel transport described in Subsection 3.2. Here $\mathcal{K}_n^{-1} \cdots \mathcal{K}_1^{-1}$ denotes a sequence of (inverse) $\mathcal{K}$-wall jumps of the network, corresponding precisely to the flips in κ, ordered from right to left. A $\mathcal{K}$ wall corresponding to a mutation on node k acts on the X_γ as follows

$$(27) \qquad \mathcal{K}^{-1}(X_\gamma) = X_\gamma (1 + X_{-\gamma_k})^{\langle \gamma_k, \gamma \rangle}.$$

Note the appearance of $-\gamma_k$ as opposed to γ_k, this is because the $\mathcal{K}$-wall jump involves the edge of the new BPS graph *after* the flip, see Figures 7 and 8 and equation (19). Combining this identity with (25) gives

$$(28) \qquad \mathrm{Tr}F(\wp', \overline{\mathcal{G}}) = \sum_{\mathbf{c}} \overline{\Omega}(\overline{\mathcal{G}}, \gamma, \wp)\, \mathcal{K}_1 \cdots \mathcal{K}_n \left(X_{\kappa(\gamma)} \right).$$

We would like to express the r.h.s. in terms of the holonomy $\mathrm{Tr}F(\wp, \overline{\mathcal{G}})$. In order to achieve that, we first need a technical result, whose proof can be found in Appendix A. Introduce a map ρ defined as follows

$$(29) \qquad \rho_{\mathcal{G}} : X_{\gamma_i} \to y_i,$$

this definition is formulated in terms of the basis elements of the initial BPS graph $\mathcal{G}$ and its cluster variables y_i. ρ extends to other homology classes by multiplication $X_{\gamma + \gamma'} = X_\gamma X_{\gamma'}$. We claim that

$$(30) \qquad \mathcal{K}_1 \ldots \mathcal{K}_n(X_{\kappa(\gamma_i)}) = \rho^{-1} \circ \kappa \circ \rho(X_{\gamma_i}),$$

where $\mathcal{K}_1 \ldots \mathcal{K}_n$ is a sequence of $\mathcal{K}$-wall transformations, applied in the *opposite* order compared to how they occur on the BPS graph ($\mathcal{K}_1$ happens first, but its transformation is applied last).

Using this result in (28) gives

$$(31) \qquad \mathrm{Tr}F(\wp', \overline{\mathcal{G}}) = \sum_{\mathbf{c}} \overline{\Omega}(\overline{\mathcal{G}}, \gamma, \wp)\, \rho^{-1} \circ \kappa \circ \rho \left(X_\gamma \right).$$

Finally, we go back to cluster variables by applying ρ on each side, and come to the main result of this section

$$(32) \qquad \rho \left(\mathrm{Tr}F(\wp', \overline{\mathcal{G}}) \right) = \kappa \circ \rho \left(\mathrm{Tr}F(\wp, \overline{\mathcal{G}}) \right).$$

This identity holds for a generic sequence of moves $\kappa = \kappa_r \circ \kappa_s$ made of flips, cooties, j-moves and relabelings, provided that it corresponds to an element of $\mathrm{MCG}(C)$, subject to the consistency conditions described in Section 2.

Equation (32) shows that the action by κ on cluster variables y_i corresponds to turning the holonomy along $\wp$ into the holonomy along a new path $\wp'$. Moreover $\wp'$ and $\wp$ are related precisely by the mapping class group transformation g_κ acting on $H_1(C, \mathbb{Z})$. This relation provides strong evidence that our construction of the mapping class group via the cluster algebra and BPS graphs acts as expected on the moduli space of flat $GL(K)$ connections on C. On the other hand, if the mapping class group action generated by a BPS graph is shown to satisfy this relation, this provides evidence that $\mathcal{G}$ really arises from a degenerate spectral network.

4. Examples

In this section we work out the construction of the mapping class group in several examples, and perform several checks, including the group relations of generators of $\mathrm{MCG}(C)$ and the action on UV line operators.

4.1. $SU(2)$ $\mathcal{N} = 2^*$ theory

The $SU(2)$ gauge theory with a massive adjoint hypermultiplet is realized as a class $\mathcal{S}$ theory by taking the A_1 Hitchin system with C a torus with a regular puncture. The mapping class group action for this example does not require the machinery of BPS graphs, and has been previously studied using other techniques [4, 30, 31, 44, 45]. Nevertheless we include it both for completeness and for pedagogical purposes.
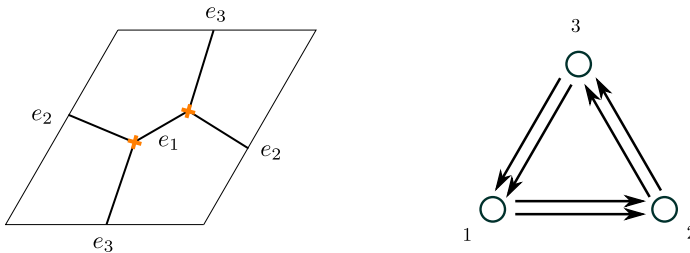

Figure 9: The BPS graph of $SU(2)$ $\mathcal{N} = 2^*$ theory, and the dual quiver.

The spectral curve has genus two and has two punctures, however the physical charge lattice is just three dimensional, as a result of a quotient [46]. The BPS graph of the theory is shown in Figure 9, it is made of three edges e_i. Each edge corresponds to an elementary web, the intersection pairing of the respective homology cycles $\gamma_i = h(e_i)$ is

$$(33) \qquad \langle \gamma_i, \gamma_{i+1} \rangle = -2.$$

Accordingly the quiver has $b_{i,i+1} = 2$ arrows connecting node i to $i+1$. Note that $\gamma_1 + \gamma_2 + \gamma_3$ is a flavor charge, it has vanishing intersection with any other cycle. We choose to represent the generators of the homology lattice of C as

$$(34) \qquad A = [(e_1, e_2)], \qquad B = [(e_1, e_3)],$$

note that the orientation of each is ambiguous, since the cyclic ordering is preserved by reversing the ordering. This is a peculiarity of the $SU(2)$ theory, and will bring specific consequences. We choose A oriented to the right, and B oriented upwards.
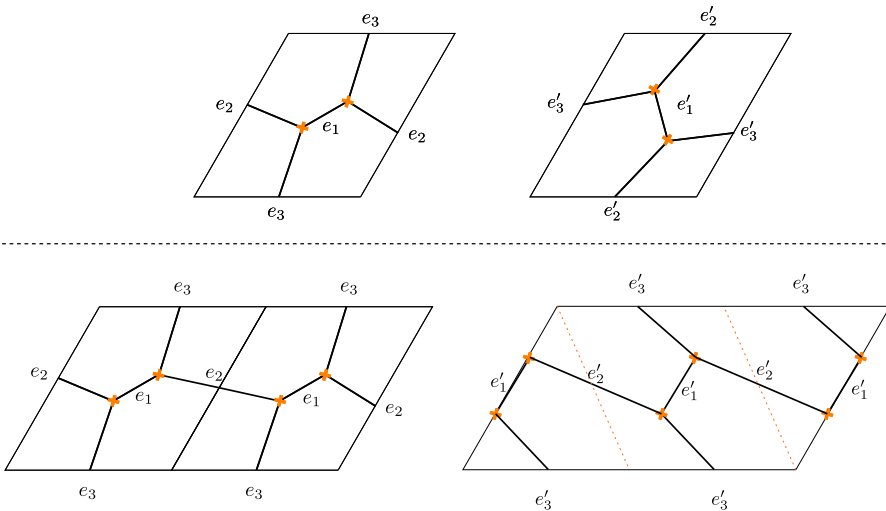

Figure 10: Top: the S^{-1} move. Bottom: the T^{-1} move.

The S^{-1} transformation is obtained by performing a single flip κ_s on edge e_1 followed by a relabeling $\kappa_r : e_2 \leftrightarrow e_3$, see Figure 10. As a check, note

that

$$(35) \qquad A' = [(e'_1, e'_2)] = B, \qquad B' = [(e'_1, e'_3)] = -A$$

which indeed corresponds to the action of S^{-1}.[15] Let us therefore denote by $\kappa_{S^{-1}} = \kappa_r \circ \kappa_s$. On the cluster variables, this transformation acts by the mutation μ_1 on node 1, followed by a permutation of nodes $2 \leftrightarrow 3$

$$(36) \qquad \kappa_{S^{-1}}(y_1, y_2, y_3) = \left(y_1^{-1}, y_3(1 + y_1^{-1})^{-2}, y_2 y_1^2 (1 + y_1^{-1})^2 \right).$$

Another generator of $\mathrm{MCG}(C)$ can be chosen to be the flip on edge e_2 followed by the permutation of $e_1 \leftrightarrow e_2$, see Figure 10. The homology basis on C gets mapped to

$$(37) \qquad A' = [(e'_1, e'_2)] = A, \qquad B' = [(e'_1, e'_3)] = B - A,$$

therefore we recognize this as the action of

$$(38) \qquad T^{-1} = \begin{pmatrix} 1 & -1 \\ 0 & 1 \end{pmatrix}.$$

On the cluster variables this acts by composition of a mutation μ_2 on node 2, followed by a permutation of nodes $1 \leftrightarrow 2$

$$(39) \qquad \kappa_{T^{-1}}(y_1, y_2, y_3) = \left(y_2^{-1}, y_1(1 + y_2^{-1})^{-2}, y_3(1 + y_2)^2 \right).$$

As a check that the identifications are consistent among themselves, we can verify that the identity $\left(S^{-1} T^{-1} \right)^3 = 1$

$$(40) \qquad (y_1, y_2, y_3) \xrightarrow{\kappa_{T^{-1}}} \left(y_2^{-1}, y_1 \left(1 + y_2^{-1} \right)^{-2}, y_3 \left(1 + y_2 \right)^2 \right)$$
$$\xrightarrow{\kappa_{S^{-1}}} (y_2, y_3, y_1)$$
$$\xrightarrow{\kappa_{T^{-1}}} \left(y_3^{-1}, y_2 \left(1 + y_3^{-1} \right)^{-2}, y_1 \left(1 + y_3 \right)^2 \right)$$
$$\xrightarrow{\kappa_{S^{-1}}} (y_3, y_1, y_2)$$
$$\xrightarrow{\kappa_{T^{-1}}} \left(y_1^{-1}, y_3 \left(1 + y_1^{-1} \right)^{-2}, y_2 \left(1 + y_1 \right)^2 \right)$$
$$\xrightarrow{\kappa_{S^{-1}}} (y_1, y_2, y_3).$$

It is also straightforward to check that $(S^{-1})^2 = 1$, this suggests that we found a representation of the orientation-preserving mapping class group

---

[15]We chose A' oriented upwards, and B' oriented left, preserving the relative orientation of A, B.

$PSL(2, \mathbb{Z})$ (as opposed to its double cover $SL(2, \mathbb{Z})$, which allows for orientation change). This appears to be a special feature of $N = 2$, and is due to the fact that the orientation of A and B cycles is ambiguous: each is composed of just two edges of $\mathcal{G}$, therefore their cyclic ordering is invariant under orientation reversal. This ambiguity will be absent for higher N.

Notice that the graph has an obvious $\mathbb{Z}_3$ symmetry, and this raises the possibility of choosing κ_r differently. For instance, considering the permutation $\kappa_r : e_1 \leftrightarrow e_3$ after the flip on edge e_2 would have given $A' = B - A, B' = 2A + B$. This corresponds to the transformation

$$(41) \qquad \begin{pmatrix} 1 & -2 \\ 1 & -1 \end{pmatrix} = S^{-1}T^{-1}S^{-1}T^{-2}S^{-2}.$$

Indeed, we checked that performing this transformation corresponds precisely to acting with the sequence $\kappa_{S^{-1}}\kappa_{T^{-1}}\kappa_{S^{-1}}\kappa_{T^{-1}}\kappa_{T^{-1}}\kappa_{S^{-1}}\kappa_{S^{-1}}$ on the cluster variables. This match provides a strong consistency check on the identification between mapping class group and cluster algebra. A nice property of this construction is how manifest the relation between mapping class group action and cluster algebra is. On the one hand the action on the BPS graph resembles directly that of $\mathrm{MCG}(C)$, on the other we read off directly on the dual quiver what is the corresponding cluster transformation.

4.1.1. Line operators.

We will now illustrate the action of $\mathrm{MCG}(C)$ on the UV line operators of the theory, to show how the general statements of Section 3 are realized in this theory. As a byproduct, we also work out the first computation of framed BPS states using BPS graphs, which involves some subtleties due to the occurrence of fractional charges.

Let us consider line operators labeled by the paths $\wp_A$ and $\wp_B$ in Figure 11. First of all we need to compute the holonomies along each path, which in turn requires us to compute the soliton data on the BPS graph. Recall that computing soliton data (and BPS states) requires a non-degenerate spectral network, we choose the American resolution of $\mathcal{G}$, denoted by $\overline{\mathcal{G}}$. The soliton data for the resolved network has been computed in [10] from which we borrow the results, see the reference for details on the computation.[16] Let Υ_i/Δ_i be the generating functions of up/down-going solitons on edge e_i. With the choice of branch cuts shown in Figure 11, the generating functions $\Delta_1, \Delta_2, \Upsilon_3$ count solitons of type 21 while their counterparts obtained from switching $\Delta \leftrightarrow \Upsilon$ count solitons of type 12. These generating

---

[16]Note that in the reference, the British resolution was adopted. This explains the slightly different expressions.
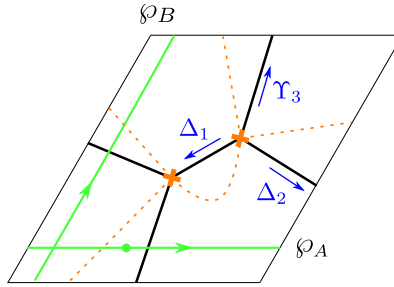
Figure 11: A choice of trivialization for the spectral curve, branch cuts are dashed lines. The cycles $\wp_A, \wp_B$ are indicated in green. Blue arrows indicate the direction of the flow of 21-walls of the spectral network arising as the American resolution of the BPS graph.

functions encode all the soliton data of the network, they are determined by the following equations

$$
(42) \qquad
\begin{array}{ll}
\underline{\text{NE}} & \underline{\text{SW}} \\
\Delta_1 = X_{a_1} + \Delta_3 & \Upsilon_1 = X_{b_1} + \Upsilon_3 \\
\Delta_2 = X_{a_2} + \Upsilon_1 & \Upsilon_2 = X_{b_2} + \Delta_1 \\
\Upsilon_3 = X_{a_3} + \Upsilon_2 & \Delta_3 = X_{b_3} + \Delta_2
\end{array}
$$

where a_i, b_i are the shortest soliton paths sourced at the NE/SW branch point, supported on edge e_i. The equations are solved by

$$
(43) \qquad
\begin{aligned}
\Delta_1 &= X_{a_1} \frac{1 + X_{\gamma_3} + X_{\gamma_2 + \gamma_3}}{1 - X_{\gamma_1 + \gamma_2 + \gamma_3}}, \\
\Upsilon_1 &= X_{b_1} \frac{1 + X_{\gamma_3} + X_{\gamma_2 + \gamma_3}}{1 - X_{\gamma_1 + \gamma_2 + \gamma_3}},
\end{aligned}
$$

and other similar expressions obtained by cyclic permutations of indices.

The formal parallel transport along the A-cycle can be computed as follows. For convenience, let us split the path into $\wp_A', \wp_A''$, with $\wp_A'$ running from the basepoint (the green dot) to the intersection with edge e_3, and $\wp_A''$ its complement. The lift of $\wp_A'$ to Σ consists of two pieces $A_1' + A_2'$, running respectively on sheets 1 and 2. $\wp_A''$ runs through a branch cut, so its lift includes two pieces $A_{12}'' + A_{21}''$, which run from sheet 1 to 2 and vice versa. The parallel transport is then computed using the standard detour rules of
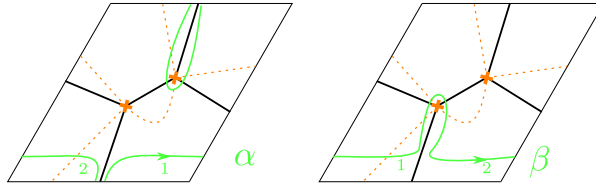
Figure 12: The paths α and β on the spectral curve Σ. Labels $1, 2$ indicate on which sheet of Σ a segment of a path lies. The sheet switches at every crossing with a branch cut (dotted lines).

spectral networks [8]

$$\mathrm{Tr}F(\wp_A, \overline{\mathcal{G}}) = \mathrm{Tr} \begin{pmatrix} X_{A'_1} & \\ & X_{A'_2} \end{pmatrix} \begin{pmatrix} 1 & \Delta_3 \\ & 1 \end{pmatrix} \begin{pmatrix} 1 & \\ \Upsilon_3 & 1 \end{pmatrix} \begin{pmatrix} & X_{A''_{12}} \\ X_{A''_{21}} & \end{pmatrix}$$

$$(44) \qquad = X_{A'_1}\Delta_3 X_{A''_{21}} + X_{A'_2}\Upsilon_3 X_{A''_{12}}.$$

To unpack this expression, consider the paths on Σ built from the concatenations $\beta = A'_1 + b_3 + A'_{21}$ and $\alpha = A'_2 + a_3 + A'_{12}$, see Figure 12. Both are closed paths, so their homology classes can be expressed in terms of the basis γ_i. By drawing representatives for these paths in our choice of trivialization, it is not hard to derive the following relations[17]

$$(45) \qquad \alpha + \beta = a_3 + b_3 = \gamma_3, \qquad \alpha - \beta = \gamma_1 + \gamma_2 + \gamma_3.$$

Taken together, these imply that α and β are actually fractional charges

$$(46) \qquad \alpha = \frac{1}{2}(\gamma_1 + \gamma_2) + \gamma_3, \qquad \beta = -\frac{1}{2}(\gamma_1 + \gamma_2).$$

There is also a crucial sign coming from spectral networks rules, which must be taken into account [8, eq. (4.1)]. This comes from the extra unit of winding

---

[17]The first relation follows immediately from the fact that $A'_1 + A'_2 + A''_{12} + A''_{21}$ is invariant under the exchange of the two sheets, and therefore is projected out of the physical charge lattice [46] (related to this, note that the period of the Seiberg-Witten 1-form would vanish along this cycle). To derive the second one, one draws representatives for $\alpha, -\beta$ and deforms each component to join each other. In order to do this, one of the paths must pass through the puncture, picking up a cycle running clockwise around its lift to sheet 1. This is equal to $\gamma_1 + \gamma_2 + \gamma_3$, and the remaining paths are homologically trivial.

of the tangent vector of the representative of α. Overall we get

$$
\text{(47)} \qquad \text{Tr} F(\wp_A, \overline{\mathcal{G}}) = (X_\beta - X_\alpha) \frac{1 + X_{\gamma_2} + X_{\gamma_1 + \gamma_2}}{1 - X_{\gamma_1 + \gamma_2 + \gamma_3}}
$$

$$
= X_\beta (1 - X_{\alpha - \beta}) \frac{1 + X_{\gamma_2} + X_{\gamma_1 + \gamma_2}}{1 - X_{\gamma_1 + \gamma_2 + \gamma_3}}
$$

$$
= X_{-\frac{1}{2}(\gamma_1 + \gamma_2)} + X_{\frac{1}{2}(\gamma_2 - \gamma_1)} + X_{\frac{1}{2}(\gamma_1 + \gamma_2)}.
$$

This result agrees with previous computations such as [6, eq. (10.46)].

A similar computation can be done for the B-cycle line operator, and we find

$$
\text{Tr} F(\wp_B, \overline{\mathcal{G}}) = \text{Tr} \begin{pmatrix} X_{B_1'} & \\ & X_{B_2'} \end{pmatrix} \begin{pmatrix} 1 & \\ \Delta_2 & 1 \end{pmatrix} \begin{pmatrix} 1 & \Upsilon_2 \\ & 1 \end{pmatrix} \begin{pmatrix} & X_{B_{12}''} \\ X_{B_{21}''} & \end{pmatrix}
$$

$$
\text{(48)} \qquad = X_{-\frac{1}{2}(\gamma_1 + \gamma_3)} + X_{\frac{1}{2}(\gamma_1 - \gamma_3)} + X_{\frac{1}{2}(\gamma_1 + \gamma_3)}.
$$

We can now test the action of the S^{-1} generator derived in (36) according to our formula (32). Translating holonomies into cluster variables using the map ρ in (29), we find

$$
\text{(49)} \qquad \kappa_{S^{-1}} \circ \rho \left(\text{Tr} F(\wp_A, \overline{\mathcal{G}}) \right) = \kappa_{S^{-1}} \left(\frac{1}{\sqrt{y_1 y_2}} + \sqrt{\frac{y_2}{y_1}} + \sqrt{y_1 y_2} \right)
$$

$$
= \frac{1 + y_1}{\sqrt{y_1 y_3}} + \frac{\sqrt{y_1^3 y_3}}{1 + y_1} + \frac{\sqrt{y_1 y_3}}{1 + y_1}
$$

$$
= \frac{1}{\sqrt{y_1 y_3}} + \sqrt{\frac{y_1}{y_3}} + \sqrt{y_1 y_3}
$$

$$
= \rho \left(\text{Tr} F(\wp_B, \overline{\mathcal{G}}) \right)
$$

as expected, since S^{-1} takes the A cycle into the B cycle.

4.2. $SU(3)$ $\mathcal{N} = 2^*$ theory

We now move on to higher rank, and consider the class $\mathcal{S}$ theory corresponding to an A_2 Hitchin system on a punctured torus with a minimal (a.k.a. simple) puncture. In order to obtain the BPS graph we adopt a procedure described in [9]. Let $\mathcal{G}_0$ be BPS graph of the theory with a *full* puncture, this is conjectured to be dual to a 3-triangulation of the torus, see Figure 13. In order to obtain the BPS graph for the simple puncture, we consider a deformation of the mass moduli so as to partially close the puncture. This operation is expected to change the shape of the spectral network underlying

the BPS graph in a precise way, which we can mimic using the standard flip, cootie and j-move on $\mathcal{G}_0$. The deformation of $\mathcal{G}_0$ corresponds to the reduction of the puncture shown in Figure 13, and the resulting graph coincides with the one we encountered in Figure 4. Note that $\mathcal{G}$ has a $\mathbb{Z}_3$ symmetry generated by shifting labels $\gamma_1 \to \gamma_5 \to \gamma_3$ and by simultaneously rotating the webs of γ_2 and γ_4 counter-clockwise by $2\pi/3$, so as to preserve the branch point at which γ_1 meets γ_2 and γ_4, and so on. The elementary webs of $\mathcal{G}$ and their respective lifts to homology classes on Σ are

$$(50) \qquad \begin{array}{ccc} \gamma_1 = h(e_2), & \gamma_2 = h(e_4, e_5, e_6), & \gamma_3 = h(e_1), \\ \gamma_4 = h(e_7, e_8, e_9), & \gamma_5 = h(e_3). & \end{array}$$

The dual quiver is shown in Figure 5, note that it inherits the $\mathbb{Z}_3$ symmetry of $\mathcal{G}$.[18]
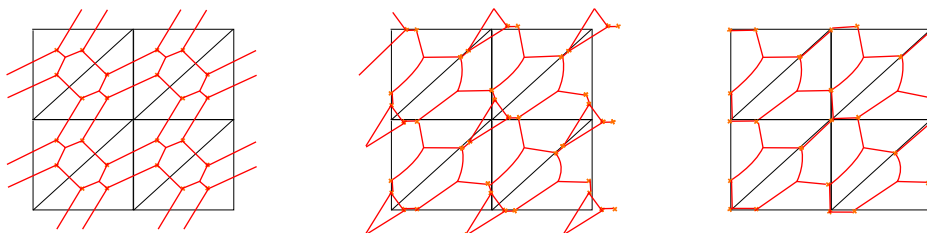

Figure 13: Left: the BPS graph for the torus with a full puncture. Center: an equivalent BPS graph obtained by performing flips. Right: the BPS graph for the torus with a $[2, 1]$ puncture, after reduction.

In order to study the mapping class group let us fix A, B cycles as in (8). The sequence of moves that generates the S^{-1} transformation is shown in Figure 4, and reads

$$(51) \qquad \kappa_s \; : f_2 \circ f_9 \circ \mathrm{cootie}(e_5, e_6, e_7, e_8) \circ f_1 \circ f_2,$$

where f_i denotes a flip of edge e_i. The graph obtained after applying κ_s has a $\mathbb{Z}_3$ symmetry, so there are three inequivalent relabelings $\kappa_r, \kappa_r', \kappa_r''$ which turn it back into the original graph. We define κ_r as in (7), providing precisely the S^{-1} transformation of the homology basis in (10).

---

[18]This quiver is related by a sequence of mutations to the one proposed in [17].

On the cluster variables κ_s translates into a sequence of mutations, which is followed by a permutation of the nodes corresponding to κ_r:

(52)
$$\kappa_s : \quad \mu_1 \circ \mu_4 \circ \mu_3 \circ \mu_1,$$
$$\kappa_r : \quad 1 \to 3 \to 2 \to 5 \to 4 \to 1.$$

The action on the cluster variables is rather involved

(53)
$$y_1' = y_3 \left(1 + y_1 \left(1 + y_3\right)\right)$$
$$\times \left(1 + y_1 2 \left(1 + y_3\right) + y_1^2 \left(1 + y_3\right) \left(1 + y_3 \left(1 + y_4\right)\right)\right)^{-1},$$
$$y_2' = y_1^3 y_3^2 y_4^2 \left(1 + y_1 \left(2 + y_3 + 2\right) + y_1^2 \left(1 + y_3 \left(1 + y_4\right)\right)\right)^{-1}$$
$$\times \left(1 + 2 y_1 \left(y_3 + 1\right) + y_1^2 \left(1 + y_3\right) \left(1 + y_3 \left(1 + y_4\right)\right)\right)^{-1},$$
$$y_3' = \left(1 + y_1 \left(1 + y_3\right)\right) \left(1 + y_1 \left(2 + y_3\right) + y_1^2 \left(1 + y_3 \left(1 + y_4\right)\right)\right) y_1^{-2} y_3^{-2} y_4^{-1},$$
$$y_4' = y_5 \Big(1 + y_1 \left(4 + 3 y_3\right) + y_1^2 \left(2 + y_3\right) \left(3 + y_3 \left(3 + y_4\right)\right)$$
$$+ y_1^3 \left(4 + 5 y_3 + y_3^2\right) \left(1 + y_3 \left(1 + y_4\right)\right) + y_1^4 \left(1 + y_3\right) \left(1 + y_3 \left(1 + y_4\right)\right)^2 \Big)$$
$$\times \left(\left(1 + y_1 \left(1 + y_3\right)\right)^3\right)^{-1},$$
$$y_5' = y_2 \left(1 + y_1 \left(1 + y_3\right)\right) \left(1 + 2 y_1 \left(1 + y_3\right) + y_1^2 \left(1 + y_3\right) \left(1 + y_3 \left(1 + y_4\right)\right)\right)$$
$$\times \left(1 + y_1 \left(2 + y_3\right) + y_1^2 \left(1 + y_3 \left(1 + y_4\right)\right)\right)^{-1}.$$

We also found a sequence of moves that corresponds to the L generator of the MCG(C). In this case the sequence of flips and cooties κ_s is shown in Figure 14. We choose a relabeling of edges κ_r which is

(54)
$$\kappa_r : \quad e_1 \to e_4 \to e_5 \to e_2 \to e_9 \to e_7 \to e_3 \to e_1.$$

The homology basis changes as follows

(55)
$$A' = A + B, \qquad B' = B,$$

implying that the complex structure of the torus transforms precisely by the transformation

(56)
$$L = \begin{pmatrix} 1 & 0 \\ 1 & 1 \end{pmatrix}.$$

The action on cluster variables is $\kappa_r \circ \kappa_s$ with

(57)
$$\begin{aligned} \kappa_s: & \quad \mu_5 \circ \mu_2 \circ \mu_1 \circ \mu_5, \\ \kappa_r: & \quad 1 \to 4 \to 5 \to 3 \to 2 \to 1, \end{aligned}$$

acting as follows

(58)
$$y_1' = y_1 \left(1 + y_5 \left(1 + y_1\right)\right)^{-1} \left(1 + y_2 \left(1 + y_1\right) \left(1 + y_5 \left(1 + y_1\right)\right)\right)^{-1},$$
$$y_2' = y_1 y_2^2 y_3 \left(1 + y_5 \left(1 + y_1\right)\right)^3 \left(1 + y_2 \left(1 + y_1\right) \left(1 + y_5 \left(1 + y_1\right)\right)\right)^{-1}$$
$$\times \left(1 + y_5 + y_2 \left(1 + y_5 \left(1 + y_1\right)\right)^2\right)^{-1},$$
$$y_3' = \left(1 + y_5 + y_2 \left(1 + y_5 \left(1 + y_1\right)\right)^2\right) \left(y_1 y_2 \left(1 + y_5 \left(1 + y_1\right)\right)\right)^{-1},$$
$$y_4' = y_1^{-1} y_5^{-1} \Big(1 + y_5 + y_2 \left(2 \left(1 + y_5\right)^2 + y_1 \left(1 + 5 y_5 + 4 y_5^2\right) + y_5 y_1^2 \left(1 + 2 y_5\right)\right)$$
$$+ y_2^2 \left(1 + y_1\right) \left(1 + y_5 \left(1 + y_1\right)\right)^3 \Big),$$
$$y_5' = y_1 y_4 y_5^2 \left(1 + y_2 \left(1 + y_1\right) \left(1 + y_5 \left(1 + y_1\right)\right)\right)$$
$$\times \left(1 + y_5 \left(1 + y_1\right)\right)^{-1} \left(1 + y_5 + y_2 \left(1 + y_5 \left(1 + y_1\right)\right)^2\right)^{-1}.$$

We checked that the $SL(2, \mathbb{Z})$ identities

(59)
$$\left(LS^{-1}\right)^3 = 1, \qquad \left(S^{-1}\right)^4 = 1,$$

are indeed satisfied by (53) and (58). Unlike for the case of $N = 2$, now there is no ambiguity in the orientation of the A, B cycles, simply because they are composed of more than two edges each. In fact, we find that $(S^{-1})^2 \neq 1$ in this case, and we have the representation of the mapping class group $SL(2, \mathbb{Z})$.

4.3. $SU(N)$ $\mathcal{N} = 2^*$ theory

We wish to generalize the analysis of the previous two subsections to punctured tori with a simple puncture, for Lie algebra A_{N-1}. Finding the BPS graph of these models in full generality is rather challenging, even resorting to the puncture-reduction techniques illustrated in the previous subsection.[19]

---

[19] We were able to obtain the BPS graph for the torus with a $[3, 1]$ puncture by reducing the BPS graph for the full puncture. We also checked that it is related to the guess of Figure 15 by a sequence of flips and cooties.
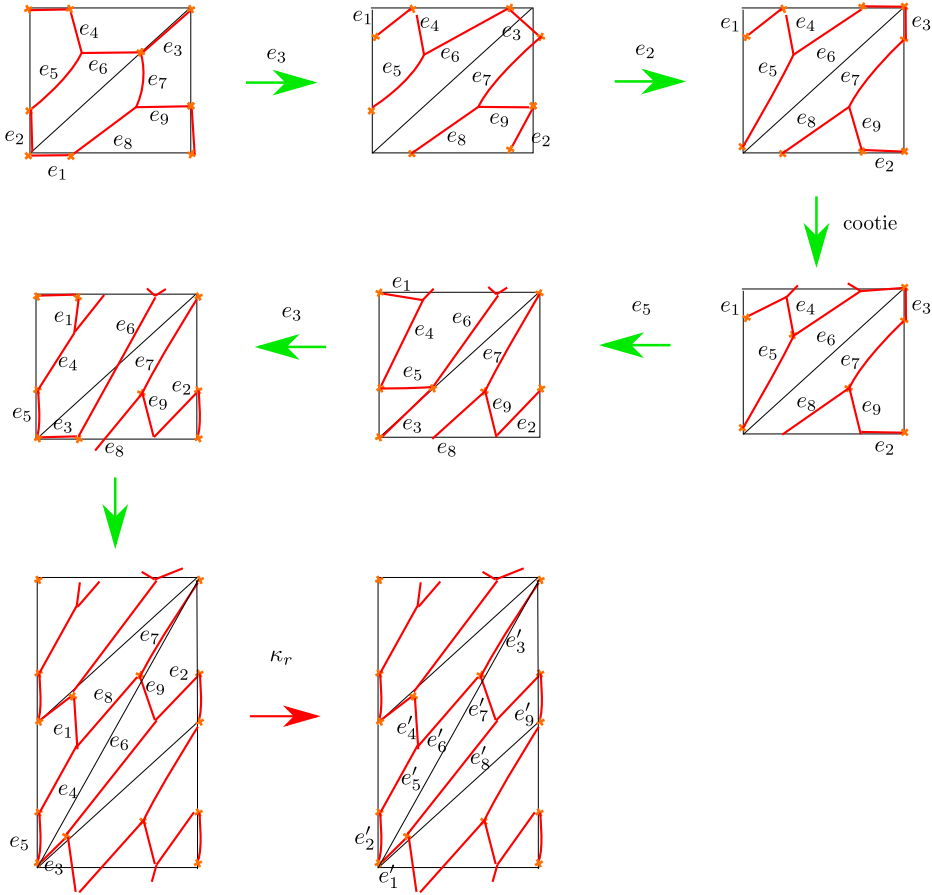
Figure 14: The L-move for the $[2, 1]$-punctured torus.

On the other hand we were able to find a natural a guess for the BPS graphs of these theories, for general N (this is supported by a heuristic argument presented in Appendix B, which also can deal with more general punctures of type $[k, 1, \ldots, 1]$). The graph and the dual quiver are shown in Figure 15. The complex dimension of the Coulomb branch is $N - 1$ while the flavor symmetry is $U(1)$, therefore the charge lattice has rank $2N - 1$, and this coincides with the elementary webs of $\mathcal{G}$. The quiver agrees in fact with previous proposals [17, 34] and, in the case of $N = 3$ it is mutation-equivalent to the one in Figure 5. We tested our guess by using the BPS graphs to derive generators of the mapping class group, and checking that

they produce consistent representations of MCG(C) on the cluster algebra for $N = 3, 4, 5$.
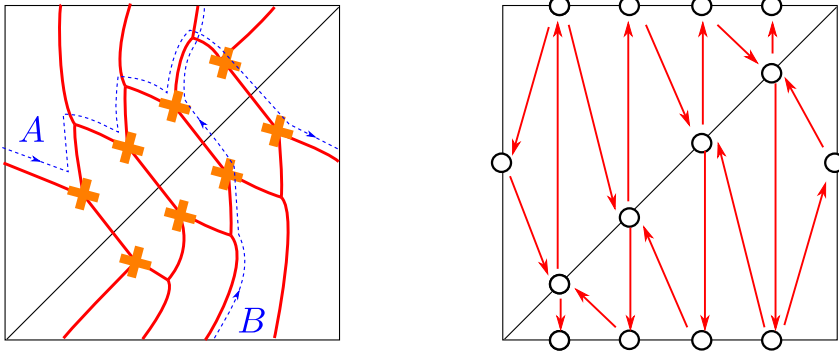
Figure 15: BPS graph for the torus with a $[N-1, 1]$ puncture, and the dual quiver. There are $N-1$ nodes on the horizontal and diagonal edges.

The A and B cycles are defined as oriented sequences of edges, depicted by dashed lines in Figure 15. We were able to find a sequence of moves κ_s that corresponds to the element L of the mapping class group. The dual sequence of mutations is

$$(60) \qquad \kappa_s : \quad \prod_{i \in I_H} \mu_i,$$

where I_H is set of quiver nodes on the horizontal edge in Figure 15, and the ordering is irrelevant since these nodes are not connected by arrows. Together with these mutations, in order to obtain the L transformation, one must apply the following relabeling of quiver nodes

$$(61) \qquad \kappa_r : \quad \left\{ \gamma_i^{(H)} \leftrightarrow \gamma_i^{(D)} \right\}_{i=1,\dots,N-1},$$

where $\gamma^{(D/H)}$ denote the nodes on the diagonal/horizontal edge respectively. These nodes get exchanged with each other pairwise. The action of L on the cluster variables is

$$(62) \qquad \kappa_L = \kappa_s \circ \kappa_r.$$

Finding other generators of the mapping class group is feasible, but much more challenging. We were not able to find a general formula valid

for all N, but for the cases $N = 3, 4, 5$ we found several possible choices for a second generator of MCG(C). They are reported in the tables below, where labels refer to Figure 16. Of course, there may be several mutations corresponding to a single a MCG transformation, and they should all be equivalent (for example, via wall-crossing identities). In writing the data we adopt the convention that parentheses $(\mu_a \circ \mu_b)$ stand for either $\mu_a \circ \mu_b$ or $\mu_b \circ \mu_a$, when the ordering does not matter.
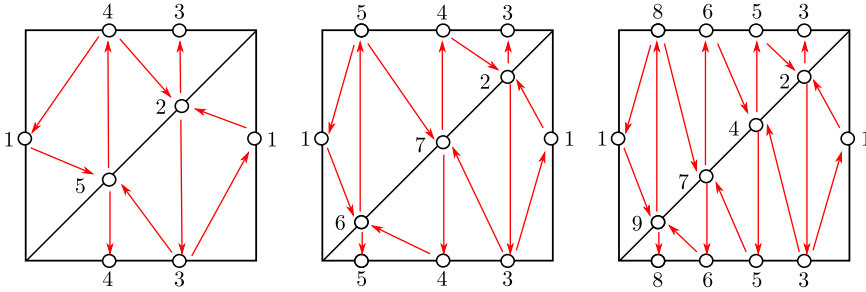
Figure 16: BPS quivers for the torus with a minimal puncture, for $N = 3, 4, 5$.

$N = 3$		
S	$\begin{pmatrix} 0 & 1 \\ -1 & 0 \end{pmatrix}$	$\kappa_s : \mu_1$ $\kappa_r : 3 \to 5 \to 4 \to 2 \to 3$
L	$\begin{pmatrix} 1 & 0 \\ 1 & 1 \end{pmatrix}$	$\kappa_s : (\mu_3 \circ \mu_4)$ $\kappa_r : 2 \leftrightarrow 3, \ 4 \leftrightarrow 5$
LS	$\begin{pmatrix} 0 & 1 \\ -1 & 1 \end{pmatrix}$	$\kappa_s : (\mu_2 \circ \mu_5) \circ \mu_1$ $\kappa_r : 2 \leftrightarrow 5$
$LS^{-1}L^{-1}$	$\begin{pmatrix} 1 & -1 \\ 2 & -1 \end{pmatrix}$	$\kappa_s : (\mu_3 \circ \mu_4) \circ \mu_1 \circ (\mu_2 \circ \mu_5)$ $\kappa_r : 2 \to 3 \to 5 \to 4 \to 2$
$S^{-1}L^{-1}$	$\begin{pmatrix} 1 & -1 \\ 1 & 0 \end{pmatrix}$	$\kappa_s : \mu_1 \circ (\mu_2 \circ \mu_5)$ $\kappa_r : 3 \leftrightarrow 4$
$L^{-1}S^{-1}$	$\begin{pmatrix} 0 & -1 \\ 1 & 1 \end{pmatrix}$	$\kappa_s : (\mu_3 \circ \mu_4) \circ \mu_1$ $\kappa_r : 2 \leftrightarrow 5$
SL	$\begin{pmatrix} 1 & 1 \\ -1 & 0 \end{pmatrix}$	$\kappa_s : \mu_1 \circ (\mu_3 \circ \mu_4)$ $\kappa_r : 2 \leftrightarrow 5$

$N = 4$		
S	$\begin{pmatrix} 0 & 1 \\ -1 & 0 \end{pmatrix}$	$\kappa_s : \mu_1 \circ \mu_4 \circ \mu_2 \circ \mu_6 \circ \mu_4 \circ \mu_5 \circ \mu_3 \circ \mu_1$ $\kappa_r : 1 \leftrightarrow 4, \ 2 \to 5 \to 6 \to 3 \to 2$
L	$\begin{pmatrix} 1 & 0 \\ 1 & 1 \end{pmatrix}$	$\kappa_s : (\mu_3 \circ \mu_5 \circ \mu_4)$ $\kappa_r : 2 \leftrightarrow 3, \ 4 \leftrightarrow 7, \ 5 \leftrightarrow 6$
LS	$\begin{pmatrix} 0 & 1 \\ -1 & 1 \end{pmatrix}$	$\kappa_s : \mu_4 \circ (\mu_2 \circ \mu_6) \circ (\mu_3 \circ \mu_5) \circ \mu_1$ $\kappa_r : 1 \to 7 \to 4 \to 1$
$LS^{-1}L^{-1}$	$\begin{pmatrix} 1 & -1 \\ 2 & -1 \end{pmatrix}$	$\kappa_s : \mu_1 \circ \mu_7 \circ (\mu_3 \circ \mu_5) \circ (\mu_2 \circ \mu_6) \circ \mu_7 \circ \mu_1$ $\kappa_r : 1 \leftrightarrow 7, \ 2 \to 3 \to 6 \to 5 \to 2$
$S^{-1}L^{-1}$	$\begin{pmatrix} 1 & -1 \\ 1 & 0 \end{pmatrix}$	$\kappa_s : \mu_7 \circ (\mu_3 \circ \mu_5) \circ (\mu_2 \circ \mu_6) \circ \mu_1$ $\kappa_r : 1 \to 4 \to 7 \to 1$

$N = 5$		
S	$\begin{pmatrix} 0 & 1 \\ -1 & 0 \end{pmatrix}$	$\kappa_s :$ $\mu_4 \circ \mu_1 \circ \mu_2 \circ \mu_9 \circ \mu_3 \circ \mu_2 \circ \mu_6$ $\circ \mu_5 \circ \mu_4 \circ \mu_1 \circ \mu_9 \circ \mu_2 \circ \mu_7 \circ \mu_4$ $\circ \mu_8 \circ \mu_1 \circ \mu_9 \circ \mu_2 \circ \mu_7 \circ \mu_8 \circ \mu_3$ $\circ \mu_1 \circ \mu_8 \circ \mu_6 \circ \mu_5 \circ \mu_1$ $\kappa_r :$ $1 \to 6 \to 2 \to 3 \to 8 \to$ $\to 7 \to 4 \to 5 \to 9 \to 1$
L	$\begin{pmatrix} 1 & 0 \\ 1 & 1 \end{pmatrix}$	$\kappa_s : (\mu_3 \circ \mu_5 \circ \mu_6 \circ \mu_8)$ $\kappa_r : 2 \leftrightarrow 3, \ 4 \leftrightarrow 5, \ 6 \leftrightarrow 7, \ 8 \leftrightarrow 9$
$L^2S^{-1}L^{-1}$	$\begin{pmatrix} 1 & -1 \\ 3 & -2 \end{pmatrix}$	$\kappa_s :$ $\mu_1 \circ \mu_2 \circ \mu_9 \circ \mu_1 \circ \mu_7 \circ \mu_4 \circ \mu_6$ $\circ \mu_5 \circ \mu_2 \circ \mu_9 \circ \mu_7 \circ \mu_4 \circ \mu_8$ $\circ \mu_3 \circ \mu_2 \circ \mu_9 \circ \mu_1$ $\kappa_r :$ $2 \leftrightarrow 9, \ 3 \to 6 \to 4 \to 3,$ $5 \to 7 \to 8 \to 5$

We checked that the cluster transformations generated by these sequences, composed with appropriate permutations of nodes, correctly reproduce the $SL(2, \mathbb{Z})$ algebra.

As explained in Section 3, if our guess for the BPS graph actually arises from a spectral network $\overline{\mathcal{G}}$, the latter could be used to compute framed BPS spectra, and our construction of $\mathrm{MCG}(C)$ would act on the moduli spaces of flat $GL(N)$ connections over C. One way to test this would be simply to draw the "completion" of $\mathcal{G}$ into a spectral network, in the spirit of *general spectral networks* [8, Section 9]. Another possibility would be to test the generators of $\mathrm{MCG}(C)$ on explicit expressions for the VEVs of UV line operators.

4.4. $SU(2)$ $N_f = 4$ theory

The $SU(2)$ gauge theory with four fundamental hypermultplets is realized as an A_1 theory of class $\mathcal{S}$ on a four-punctured sphere, with regular punctures. Its BPS graph is shown in Figure 17. $\mathcal{G}$ has six edges, each is mapped to a generator $\gamma_i = h(e_i)$ of $H_1(\Sigma, \mathbb{Z})$ with intersection pairing

$$
(63) \qquad \langle \gamma_i, \gamma_j \rangle =
\begin{pmatrix}
0 & -1 & 1 & 1 & 0 & -1 \\
1 & 0 & -1 & -1 & 1 & 0 \\
-1 & 1 & 0 & 0 & -1 & 1 \\
-1 & 1 & 0 & 0 & -1 & 1 \\
0 & -1 & 1 & 1 & 0 & -1 \\
1 & 0 & -1 & -1 & 1 & 0
\end{pmatrix} .
$$
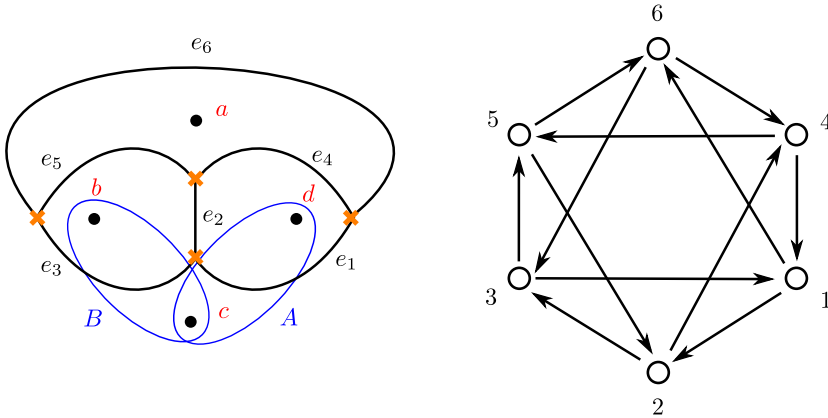
Figure 17: The BPS graph of $SU(2)$ $N_f = 4$ theory, and its quiver.

To construct the mapping class group, it will be convenient to adopt a slightly different approach than we did with the torus. Instead of working with homology cycles on C, it is simpler to introduce a system of arcs connecting the punctures, and to keep track of how they evolve under the action of MCG(C).

Performing a flip on edge e_3 followed by a flip on edge e_4, then relabeling according to

$$
(64) \qquad \kappa_r : 2 \to 3 \to 6 \to 4 \to 2
$$

produces the BPS graph of Figure 18 (to avoid clutter, we draw only two arcs). The picture is slightly deceiving, at first it appears that the BPS

graph went back to itself while the Riemann surface C was acted upon with a Dehn half-twist along the A cycle. However just the opposite happened. We should regard C as fixed, like in subsection 4.1, while the BPS graph was acted upon by an *inverse* Dehn half-twist. To obtain the full (inverse) Dehn twist we can simply apply the move twice. The action on cluster variables corresponds to a mutation on node 3, followed by a mutation on node 4 and by a permutation of nodes as in (64). The result is

$$(65) \quad \begin{aligned} &y_1' = y_1 \left(1 + y_3\right)\left(1 + y_4\right), \quad y_2' = y_4^{-1}, \\ &y_3' = y_2 y_3 y_4 \left(1+y_3\right)^{-1}\left(1+y_4\right)^{-1}, \quad y_4' = y_3 y_4 y_6 \left(1+y_3\right)^{-1}\left(1+y_4\right)^{-1}, \\ &y_5' = y_5 \left(1 + y_3\right)\left(1 + y_4\right), \quad y_6' = y_3^{-1}. \end{aligned}$$
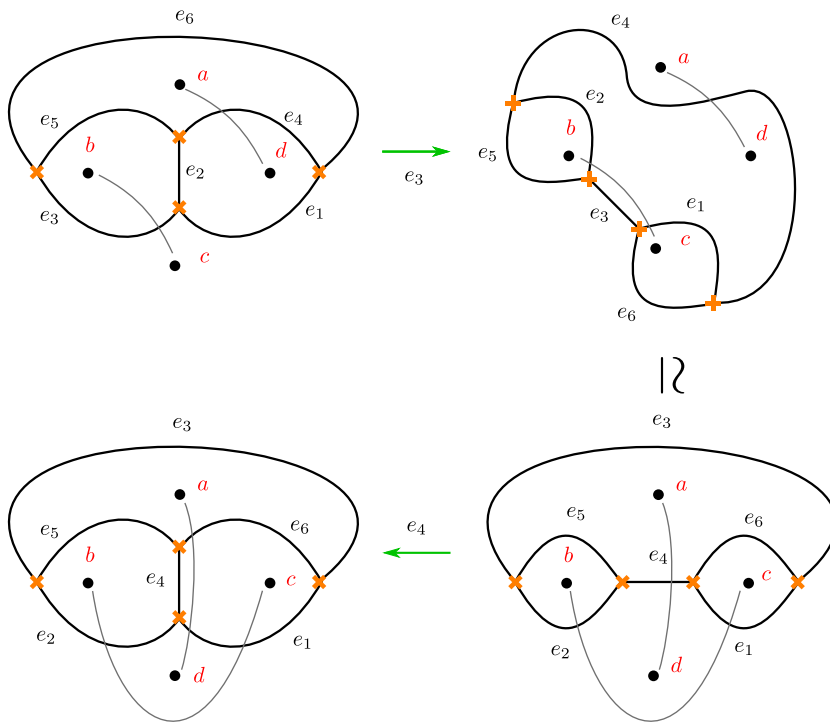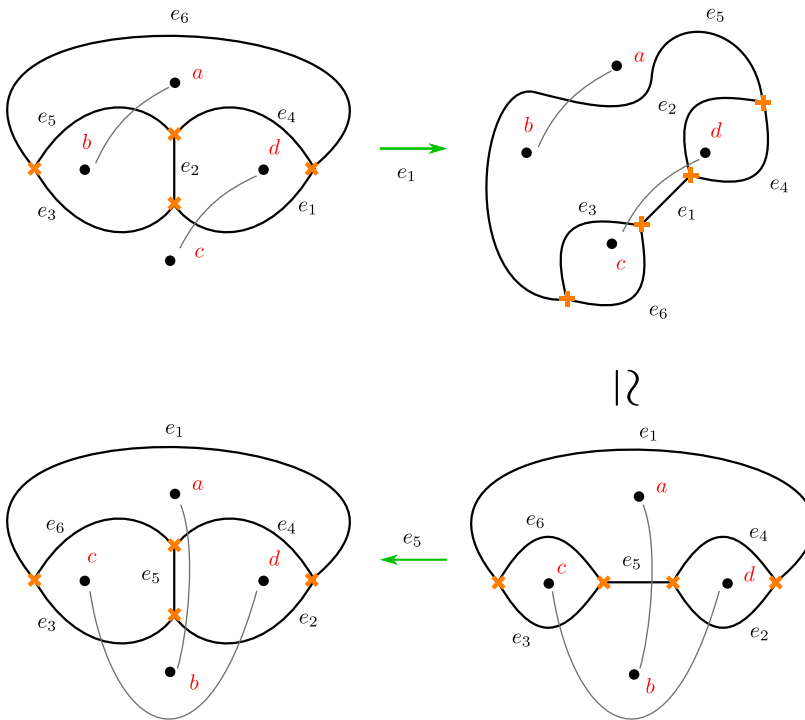

Figure 18: A half Dehn twist along the A cycle on C exchanges punctures $c \leftrightarrow d$. In our setup however this should be thought as keeping punctures fixed, and acting the the inverse half-twist on $\mathcal{G}$.

It is straightforward to generate other Dehn twists, by using the symmetries of $\mathcal{G}$ viewed as a tetrahedron. For example, a twist around the B-cycle

can be generated by flipping edge e_1 and subsequently edge e_5, then relabeling according to

$$(66) \qquad \kappa_r : 1 \to 6 \to 5 \to 2 \to 1.$$

This produces the inverse of a half-Dehn twist along the B-cycle, see Figure 19. The action on cluster variables in this case is

$$(67) \quad \begin{aligned} &y_1' = y_2 \left(1 + y_1\right)\left(1 + y_5\right), \quad y_2' = y_5^{-1}, \\ &y_3' = y_1 y_3 y_5 \left(1 + y_1\right)^{-1}\left(1 + y_5\right)^{-1}, \quad y_4' = y_1 y_4 y_5 \left(1 + y_1\right)^{-1}\left(1 + y_5\right)^{-1}, \\ &y_5' = y_6 \left(1 + y_1\right)\left(1 + y_5\right), \quad y_6' = y_1^{-1}. \end{aligned}$$

Figure 19: An inverse half Dehn twist along the B cycle exchanges punctures $b \leftrightarrow c$. In our setup however this should be thought as keeping punctures fixed, and acting the the positive half-twist on $\mathcal{G}$.

4.4.1. Line operators. Consider a line operator labeled by a path $\wp_{bd}$ circling counterclockwise punctures b and d, as shown in Figure 20. The cycle $\wp_{bd}$ crosses only edge e_2, therefore we only need the generating functions Υ_2, Δ_2 of solitons running up/down on this edge. The resolved spectral network underlying $\mathcal{G}$ will be denoted by $\overline{\mathcal{G}}$ as usual. Since we are working in the American resolution, Υ_2 is the soliton data of the oriented edge that runs upward *on the right*. Let a_2, b_2 be the solitons sourced at the upper/lower branch points of edge e_2, and define $\hat{\Upsilon}, \hat{\Delta}$ by

$$(68) \qquad \Upsilon = X_{b_2}\hat{\Upsilon}_2, \qquad \Delta = X_{b_2}\hat{\Delta}_2.$$

These reduced generating functions are readily obtained[20] using the soliton rules for the spectral network $\overline{\mathcal{G}}$ obtained by resolving $\mathcal{G}$ [10]

$$(69) \qquad \begin{aligned} \hat{\Upsilon}_2 &= \frac{1 + X_{\gamma_1}\left(1 + X_{\gamma_4}\right)}{1 - X_{\gamma_1+\gamma_2+\gamma_4}}, \\ \hat{\Delta}_2 &= \frac{1 + X_{\gamma_5}\left(1 + X_{\gamma_3}\right)}{1 - X_{\gamma_2+\gamma_3+\gamma_5}}. \end{aligned}$$
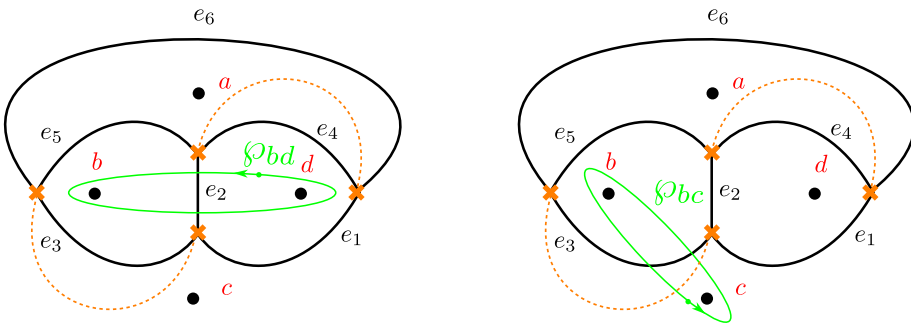

Figure 20: Left: The path $\wp_{bd}$ labeling a line operator. Right: The path $\wp_{bc}$ obtained from $\wp_{bd}$ after a half Dehn twist around the A-cycle.

With the choice of trivialization of Figure 20, the solitons encoded by Υ_2 are of type 21, while those in Δ_2 are of type 12. Let us split $\wp_{bd} = \wp'\wp''\wp'''$ into three segments, running respectively from the basepoint to the

---

[20]The computation of soliton data is nearly identical to the one detailed in [10, Section 4.7], with one important difference: here we are working with the *American* resolution of the BPS graph.

first intersection with e_2, between the two intersections with e_2, and from the second intersection with e_2 back to the basepoint. The formal parallel transport around $\wp_{bd}$ is

$$
(70) \qquad \mathrm{Tr}F(\wp_{bd}, \overline{\mathcal{G}}) = \mathrm{Tr}\left[\begin{pmatrix} X_{\wp_1'} & \\ & X_{\wp_2'} \end{pmatrix} \begin{pmatrix} 1 & \\ \Upsilon_2 & 1 \end{pmatrix} \right.
$$
$$
\begin{pmatrix} 1 & \Delta_2 \\ & 1 \end{pmatrix} \begin{pmatrix} X_{\wp_1''} & \\ & X_{\wp_2''} \end{pmatrix}
$$
$$
\left. \begin{pmatrix} 1 & \Delta_2 \\ & 1 \end{pmatrix} \begin{pmatrix} 1 & \\ \Upsilon_2 & 1 \end{pmatrix} \begin{pmatrix} X_{\wp_1'''} & \\ & X_{\wp_2'''} \end{pmatrix} \right]
$$
$$
= X_{\alpha_1} + X_{\alpha_2} + \hat{\Upsilon}_2\hat{\Delta}_2 \left(X_{\alpha_3} - X_{\alpha_4} - X_{\alpha_5} + X_{\alpha_6} \right),
$$

where the negative signs arise from from spectral networks rules, see [8, eq. (4.1)].[21] The cycles $\alpha_1 \ldots \alpha_6$ are shown in Figure 21, a tedious but simple inspection of each of them shows that

$$
(71) \quad \begin{aligned} &\alpha_1 = \tfrac{1}{2}\left(\gamma_3 + \gamma_5 - \gamma_1 - \gamma_4\right), \quad \alpha_2 = \tfrac{1}{2}\left(\gamma_1 + \gamma_4 - \gamma_3 - \gamma_5\right), \\ &\alpha_3 = -\tfrac{1}{2}\left(\gamma_1 + \gamma_4 + \gamma_3 + \gamma_5\right), \quad \alpha_4 = \tfrac{1}{2}\left(2\gamma_2 + \gamma_3 + \gamma_5 - \gamma_1 - \gamma_4\right), \\ &\alpha_5 = \tfrac{1}{2}\left(2\gamma_2 + \gamma_1 + \gamma_4 - \gamma_3 - \gamma_5\right), \quad \alpha_6 = \tfrac{1}{2}\left(4\gamma_2 + \gamma_1 + \gamma_4 + \gamma_3 + \gamma_5\right). \end{aligned}
$$

Plugging these into (70) we find

$$
(72) \qquad \mathrm{Tr}F(\wp_{bd}, \overline{\mathcal{G}}) = X_{-\frac{1}{2}(\gamma_1 + \gamma_3 + \gamma_4 + \gamma_5)}
$$
$$
\times \left(1 + X_{\gamma_1} + X_{\gamma_5} + X_{\gamma_1 + \gamma_5} \right.
$$
$$
\left. + X_{\gamma_1 + \gamma_4 + \gamma_5} + X_{\gamma_1 + \gamma_3 + \gamma_5} + X_{\gamma_1 + \gamma_3 + \gamma_4 + \gamma_5} \right).
$$

This expression matches with previous computations, see [6, eq. (10.44)].

Next we would like to check the action of the mapping class group on $\mathrm{Tr}F(\wp_{bd}, \overline{\mathcal{G}})$. Acting with a positive Dehn half-twist around the A-cycle turns $\wp_{bd}$ into $\wp_{bc}$ shown in Figure 20. It is now important to recall the subtlety involved in Figure 18: the sequence of moves depicted there corresponds to the *inverse* half-twist. In order to get the positive half twist we act on the holonomy with the inverse of (65), that is

$$
(73) \qquad\qquad\qquad \kappa_{D_A} \equiv \mu_3 \circ \mu_4 \circ \kappa_r^{-1}.
$$

---

[21]These signs count the winding of the tangent vector to each path α_i mod 2. In our example, they show up in α_4, α_5 as can be seen from Figure 21.
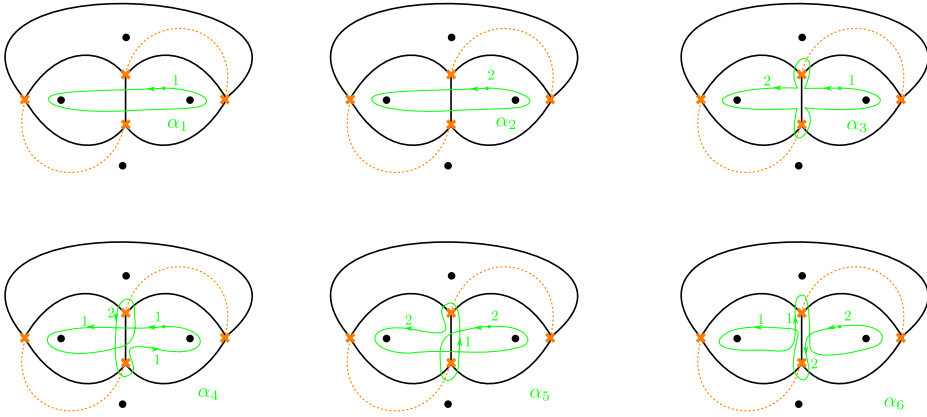
Figure 21: The cycles $\alpha_1 \ldots \alpha_6$. The numbers $1, 2$ near each path specify on which sheet of Σ the path is running.

This map acts on cluster variables as follows

$$
(74) \quad
\begin{aligned}
&y_1' = y_1 y_2 y_6 (1 + y_2)^{-1} (1 + y_6)^{-1}, \quad y_2' = y_3 (1 + y_2) (1 + y_6), \\
&y_3' = y_6^{-1}, \quad y_4' = y_2^{-1}, \quad y_5' = y_2 y_5 y_6 (1 + y_2)^{-1} (1 + y_6)^{-1}, \\
&y_6' = y_4 (1 + y_2) (1 + y_6).
\end{aligned}
$$

Using the map (29) allows to rewrite the holonomy in terms of cluster variables, then acting with the coordinate transformation (74) gives

$$
\begin{aligned}
(75) \quad \kappa_{D_A} \circ \rho \left(\operatorname{Tr} F(\wp_{bd}, \overline{\mathcal{G}}) \right) = \kappa_{D_A} &\left(\frac{1}{\sqrt{y_1 y_3 y_4 y_5}} + \sqrt{\frac{y_1}{y_3 y_4 y_5}} \right. \\
&+ \sqrt{\frac{y_5}{y_1 y_3 y_4}} + \sqrt{\frac{y_1 y_5}{y_3 y_4}} \\
&\left. + \sqrt{\frac{y_1 y_4 y_5}{y_3}} + \sqrt{\frac{y_1 y_3 y_5}{y_4}} + \sqrt{y_1 y_3 y_4 y_5} \right) \\
= &\frac{1}{\sqrt{y_1 y_2 y_5 y_6}} + \sqrt{\frac{y_6}{y_1 y_2 y_5}} \\
&+ \sqrt{\frac{y_2}{y_1 y_5 y_6}} + \sqrt{\frac{y_2 y_6}{y_1 y_5}} \\
&+ \sqrt{\frac{y_1 y_2 y_6}{y_5}} + \sqrt{\frac{y_2 y_5 y_6}{y_1}} + \sqrt{y_1 y_2 y_5 y_6} \\
= &\rho \left(\operatorname{Tr} F(\wp_{bc}, \overline{\mathcal{G}}) \right).
\end{aligned}
$$

The last expression clearly coincides with the holonomy around $\wp_{bc}$: this is evident by simply acting on (72) with the discrete symmetries of the BPS graph, viewed as a tetrahedron.

As a further check, we may use the symmetries of the BPS graph to write down the holonomy for a cycle $\wp_{cd}$ around punctures c and d

$$(76) \qquad \mathrm{Tr} F(\wp_{cd}, \overline{\mathcal{G}}) = X_{-\frac{1}{2}(\gamma_2 + \gamma_3 + \gamma_4 + \gamma_6)}$$
$$\times \left(1 + X_{\gamma_3} + X_{\gamma_4} + X_{\gamma_3 + \gamma_4} \right.$$
$$\left. + X_{\gamma_2 + \gamma_3 + \gamma_4} + X_{\gamma_3 + \gamma_4 + \gamma_6} + X_{\gamma_2 + \gamma_3 + \gamma_4 + \gamma_6} \right).$$

It is straightforward to check that (74) leaves this holonomy invariant

$$(77) \qquad \kappa_{D_A} \circ \rho \left(\mathrm{Tr} F(\wp_{cd}, \overline{\mathcal{G}}) \right) = \rho \left(\mathrm{Tr} F(\wp_{cd}, \overline{\mathcal{G}}) \right),$$

as expected from the fact that the twist around the A-cycle leaves $\wp_{cd}$ invariant.

Acknowledgements

Appendix A. Cluster mutations and $\mathcal{K}$-walls

In this section we give a proof of the identity (30). This statement is a version of the known statement in the literature, namely the decomposition of the cluster transformation for the cluster variables into the so-called monomial part and the automorphism part [11]. We nevertheless present here the self-contained proof for completeness.

To begin with, suppose κ consists of a single flip on edge e_k of a BPS graph $\mathcal{G}$. The corresponding resolved spectral network undergoes a single $\mathcal{K}$-wall jump, which results in the following transformation on the X_γ variables

$$(A.1) \qquad \mathcal{K}_{\gamma_k'}^{-1}(X_\gamma) = X_\gamma(1 + X_{\gamma_k'})^{-\langle \gamma_k', \gamma \rangle} = X_\gamma(1 + X_{-\gamma_k})^{\langle \gamma_k, \gamma \rangle}.$$

Note the appearance of γ_k' as opposed to γ_k, this is because the $\mathcal{K}$-wall jump involves the edge of the new BPS graph *after* the flip, see Figures 7 and 8. Now we would like to compare this coordinate transformation for X_γ with the cluster transformation on the variables of the dual quiver, which is given in (15). Using the map ρ introduced in (29), the action of a single flip is, respectively, on the cluster variables and on X_γ

$$\mu_k \circ \rho(X_{\gamma_i}) = \mu_k(y_i) = y_i y_k^{[-b_{ik}]_+} \left(1 + y_k^{-1}\right)^{-b_{ik}},$$

$$(A.2) \qquad \begin{aligned} \rho \circ \mathcal{K}_{\gamma_k'}(X_{\kappa(\gamma_i)}) &= \rho \left(X_{\gamma_i'}(1 + X_{\gamma_k'})^{\langle \gamma_k', \gamma_i \rangle} \right) \\ &= \rho \left(X_{\gamma_i + \gamma_k [\langle \gamma_i, \gamma_k \rangle]_+}(1 + X_{-\gamma_k})^{-\langle \gamma_k, \gamma_i \rangle} \right) \\ &= y_i y_k^{[-b_{ik}]_+} \left(1 + y_k^{-1}\right)^{-b_{ik}}, \end{aligned}$$

where we used the following reformulation of the jump of basis charges (19)

$$(A.3) \qquad \gamma_i' = \gamma_i + \gamma_k \left[\langle \gamma_i, \gamma_k \rangle\right]_+, \qquad\qquad \gamma_k' = -\gamma_k,$$

compatibly with (14) through the relation $b_{ij} = -\langle \gamma_i, \gamma_j \rangle$. This proves (30) in the case when κ is a single flip.

Next we consider two flips. The first one, denoted by λ, is performed on edge e_ℓ, then a second one κ is performed on edge e_k. Let γ_i, y_i be the charges and cluster variables associated to the quiver nodes before acting with λ, κ. Likewise, let γ_i', y_i' be the charges and cluster variables after the flip λ, and γ_i'', y_i'' the charges and cluster variables after $\kappa \circ \lambda$. Applying definitions, the cluster variables y_i with $i \neq k, \ell$ transform as

$$(A.4) \qquad \begin{aligned} \kappa \circ \lambda(y_i) &= y_i'(y_k')^{[-b_{ik}']_+}(1 + (y_k')^{-1})^{-b_{ik}'} \\ &= y_i y_\ell^{[-b_{i\ell}]_+}(1 + y_\ell^{-1})^{-b_{i\ell}} \\ &\quad \times y_k^{[-b_{ik}']_+} y_\ell^{[-b_{ik}']_+ + [-b_{k\ell}]_+}(1 + y_\ell^{-1})^{-b_{k\ell}[-b_{ik}']_+} \\ &\quad \times \left(1 + y_k^{-1} y_\ell^{-[-b_{k\ell}]_+}(1 + y_\ell^{-1})^{b_{k\ell}}\right)^{-b_{ik}'}. \end{aligned}$$

The X_γ transform as

$$(A.5) \quad \mathcal{K}_{\gamma_\ell'} \mathcal{K}_{\gamma_k''}(X_{\gamma_i''}) = X_{\gamma_i''}(1 + X_{\gamma_\ell'})^{\langle \gamma_\ell', \gamma_i'' \rangle}(1 + X_{\gamma_k''}(1 + X_{\gamma_\ell'})^{\langle \gamma_\ell', \gamma_k'' \rangle})^{\langle \gamma_\ell', \gamma_i'' \rangle}.$$

The charges are related as follows

(A.6)
$$\gamma_i' = \gamma_i + [\langle \gamma_i, \gamma_\ell \rangle]_+ \gamma_\ell, \qquad \gamma_k' = \gamma_k + [\langle \gamma_k, \gamma_\ell \rangle]_+ \gamma_\ell,$$
$$\gamma_i'' = \gamma_i + [\langle \gamma_i, \gamma_\ell \rangle]_+ \gamma_\ell + [\langle \gamma_i', \gamma_k' \rangle]_+ \gamma_k + [\langle \gamma_i', \gamma_k' \rangle]_+ [\langle \gamma_k, \gamma_\ell \rangle]_+ \gamma_\ell.$$

Therefore we can match (A.4) and (A.5), piece by piece as follows

$$(A.7) \qquad \rho(X_{\gamma_i''}) = y_i'' = y_i y_\ell^{[-b_{i\ell}]_+} y_\ell^{[-b_{k\ell}]_+ + [-b_{ik}']_+} y_k^{[-b_{ik}']_+},$$

$$(A.8) \qquad \rho \left(1 + X_{\gamma_\ell'} \right)^{\langle \gamma_\ell', \gamma_i'' \rangle} = (1 + y_\ell^{-1})^{-b_{i\ell} - b_{k\ell}[-b_{ik}']_+},$$

and the last big parenthesis in (A.5) by noting

(A.9)
$$\langle \gamma_k'', \gamma_i'' \rangle = -b_{ik}'' = -b_{ik}',$$
$$\rho \left(X_{\gamma_k''} \right) = y_k^{-1} y_\ell^{-[-b_{k\ell}]_+},$$
$$\rho \left((1 + X_{\gamma_\ell'})^{\langle \gamma_\ell', \gamma_k'' \rangle} \right) = (1 + y_\ell^{-1})^{b_{k\ell}}.$$

This proves (30) for the case when κ consists of two flips. By induction, this proof can be extended to the case of n consecutive flips.

Last, we must deal with relabelings of edges of $\mathcal{G}$, by our conventions these are performed after all flips, cooties and j-moves. We consider $\kappa = \kappa_r \circ \kappa_s$, with a permutation κ_r. For illustration, we take $\kappa_s = \mu_k$ to be a single flip on edge e_k. κ_r acts on the basis charges associated with elementary webs simply as a permutation

$$(A.10) \qquad \kappa_r : \ \gamma_i' \mapsto \gamma_i'' = \gamma_{\kappa_r(i)}',$$

where $\kappa_r(i)$ denotes the image of node i of the dual BPS quiver (cf. (52)). On cluster variables the overall action is

$$(A.11) \qquad \kappa_r \circ \kappa_s(y_i) = \kappa_r(y_i') = y_{\kappa_r(i)}' = y_{\kappa_r(i)} y_k^{[-b_{\kappa_r(i),k}]_+} (1 + y_k^{-1})^{-b_{\kappa_r(i),k}}.$$

On the X_γ, the ordering is reversed, so κ_r must be applied before all $\mathcal{K}$-wall transformation

$$(A.12) \qquad \mathcal{K}_{\gamma_k'} \left(X_{\kappa_r \circ \kappa_s(\gamma_i)} \right) = X_{\gamma_{\kappa_r(i)}'} (1 + X_{\gamma_k'})^{\langle \gamma_k', \gamma_{\kappa_r(i)}' \rangle}$$
$$\xrightarrow{\rho} y_{\kappa_r(i)} y_k^{[-b_{\kappa_r(i),k}]_+} (1 + y_k^{-1})^{-b_{\kappa_r(i),k}}.$$

The two clearly coincide, proving that (30) behaves well also under composition of mutations with a permutation.

Appendix B. BPS graphs on once-punctured torus with a partial puncture

In this appendix we present a heuristic procedure to derive the BPS graph of the once punctured torus $C_{1,1}$, with a partial puncture of the type $[k, 1 \ldots, 1]$. Related construction has appeared previously in [34] in more combinatorial context.

Let us start by recalling the puncture reduction proposed in [9]. For our purposes it will suffice to review the case of the A_{N-1} theory on a sphere with 3 punctures $C_{0,3}$, with two full punctures and one partial puncture of the type $[k, 1 \ldots, 1]$.

We first start with the case where all the punctures are maximal. The sphere $C_{0,3}$ can be triangulated by two ideal triangles, and each triangle can be triangulated with $N(N-1)/2$ branch points, as in the left of Figure B1 (shown there for the case $N = 5$, where only one of the two triangles are shown).

The reduction from the maximal puncture to a $[k, 1 \ldots, 1]$ is done in two steps: one starts from the BPS graph corresponding to an ideal triangulation of $C_{0,3}$ with three full punctures, and then remove $k(k-1)/2$ branch points around the puncture we want to reduce. This is illustrated in Figure B1, for the case $N = 5$ and $k = 3$.
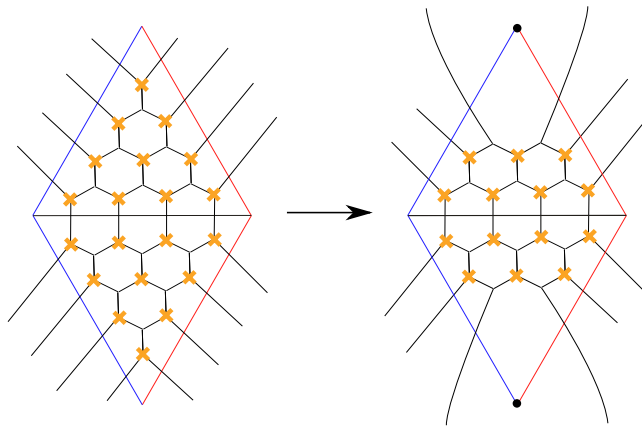

Figure B1: Reduction from the maximal puncture $[1, 1, 1, 1, 1]$ to a partial puncture $[3, 1, 1]$, for A_4 theory on a three punctured sphere $C_{0,3}$. The highlighted puncture degenerated to a partial puncture, while the other two punctures stay maximal. The two triangles are glued according to the colors of the edges.

Now, in order to apply this to obtain the torus with one partial puncture, we start from an ideal triangulation of $C_{0,3}$ with two full punctures and one reduced puncture of type $[k, 1, \ldots, 1]$ as above. We write the triangulated surface in a plane, and starting from one of the full punctures, we label the external edges as $r_1, \ldots, r_{k+1}$, $l_1, \ldots, l_{k-1}, l'_{k-1}, \ldots, l'_1$ and $r'_{k+1}, \ldots, r'_1$, see Figure B2 for an example. The identifications for the $C_{0,3}$ triangulations are

$$(B.13) \qquad r_i \approx r'_i \quad (i = 1, \ldots, k+1), \qquad l'_j \approx l'_j \quad (j = 1, \ldots, k-1).$$
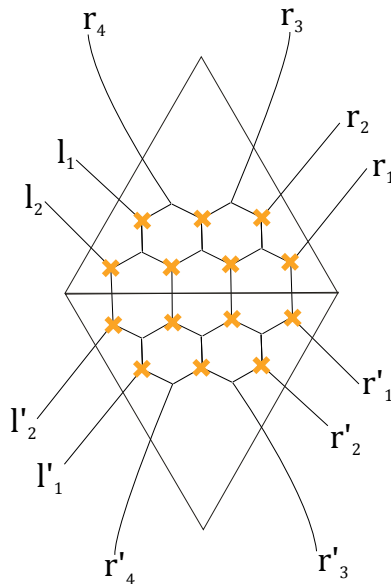

Figure B2: Ideal triangulation of $C_{0,3}$ with a $[3, 1, 1]$ puncture and two full punctures with labels on the external edges.

As pointed out in [9] $\lambda^{(i)} - \lambda^{(j)}$ remains finite at a partial puncture, for certain pairs of sheets i, j.[22] This implies that an ij trajectory of the spectral network behaves as it would at a generic point over C, i.e. it doesn't feel the presence of a puncture at all, and in particular this implies that we can move an ij edge across the puncture. We undo the identifications (B.13) and we move the edges labeled r_{k+1} and r' across the $[k, 1, \ldots, 1]$ puncture.

---

[22]This holds for the pairs of sheets i, j whose corresponding eigenvalues m_i, m_j coincide, in the residue matrix of the pole of the Higgs field of the Hitchin sysytem.

Then we make the following identifications:

(B.14)
$$r_{j+2} \approx l'_j, \quad r'_j \approx l_j \quad (j = 1, \ldots, k-1),$$
$$r_j \approx r'_{k+1-j} \quad (j = 1, 2),$$

see Figure B3. Our proposal is that this is the BPS graph of $C_{1,1}$ with a puncture of type $[k, 1, \ldots, 1]$.
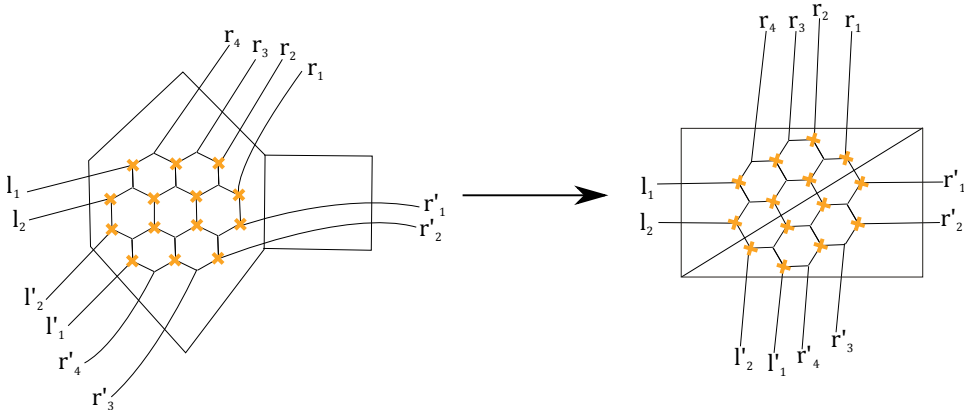

Figure B3: Adding a handle to $C_{0,3}$ by gluing two full punctures.

References

[1] D. Gaiotto, $\mathcal{N}=2$ *dualities*, JHEP **1208** (2012), 034.

[2] L. F. Alday, D. Gaiotto, and Y. Tachikawa, *Liouville correlation functions from four-dimensional gauge theories*, Lett. Math. Phys. **91** (2010), 167–197.

[3] N. Drukker, D. R. Morrison, and T. Okuda, *Loop operators and S-duality from curves on Riemann surfaces*, JHEP **09** (2009), 031.

[4] Y. Terashima and M. Yamazaki, *SL(2,R) Chern-Simons, Liouville, and gauge theory on duality walls*, JHEP **1108** (2011), 135.

[5] T. Dimofte, D. Gaiotto, and S. Gukov, *Gauge theories labelled by three-manifolds*, Commun. Math. Phys. **325** (2014), 367–419.

[6] D. Gaiotto, G. W. Moore, and A. Neitzke, *Framed BPS states*, Adv. Theor. Math. Phys. **17** (2013), 241–397.

[7] C. Córdova and A. Neitzke, *Line defects, tropicalization, and multi-centered quiver quantum mechanics*, JHEP **09** (2014), 099.

[8] D. Gaiotto, G. W. Moore, and A. Neitzke, *Spectral networks*, Annales Henri Poincaré **14** (2013), 1643–1731.

[9] M. Gabella, P. Longhi, C. Y. Park, and M. Yamazaki, *BPS graphs: From spectral networks to BPS quivers*, JHEP **07** (2017), 032.

[10] P. Longhi, *Wall-crossing invariants from spectral networks*, `arXiv: 1611.00150`.

[11] V. Fock and A. Goncharov, *Moduli spaces of local systems and higher Teichmüller theory*, Publ. Math. Inst. Hautes Études Sci. (2006), no. 103, 1–211.

[12] S. Fomin, M. Shapiro, and D. Thurston, *Cluster algebras and triangulated surfaces. I. Cluster complexes*, Acta Math. **201** (2008), no. 1, 83–146.

[13] A. Kapustin, *Wilson-'t Hooft operators in four-dimensional gauge theories and S-duality*, Phys. Rev. **D74** (2006), 025005.

[14] L. F. Alday, D. Gaiotto, S. Gukov, Y. Tachikawa, and H. Verlinde, *Loop and surface operators in $N = 2$ gauge theory and Liouville modular geometry*, JHEP **01** (2010), 113.

[15] N. Drukker, J. Gomis, T. Okuda, and J. Teschner, *Gauge theory loop operators and Liouville theory*, JHEP **02** (2010), 057.

[16] Y. Terashima and M. Yamazaki, *3d $N = 2$ theories from cluster algebras*, PTEP **2014** (2014), 023B01.

[17] D. Gang, N. Kim, M. Romo, and M. Yamazaki, *Aspects of defects in 3d-3d correspondence*, JHEP **10** (2016), 062.

[18] T. Dimofte, D. Gaiotto, and S. Gukov, 3-*manifolds and 3d indices*, Adv. Theor. Math. Phys. **17** (2013), no. 5, 975–1076.

[19] S. Lee and M. Yamazaki, *3d Chern-Simons theory from M5-branes*, JHEP **12** (2013), 035.

[20] J. Yagi, *3d TQFT from 6d SCFT*, JHEP **08** (2013), 017.

[21] C. Cordova and D. L. Jafferis, *Complex Chern-Simons from M5-branes on the squashed three-sphere*, `arXiv:1305.2891`.

[22] M. Romo, *Cluster partition function and invariants of 3-manifolds*, `arXiv:1704.00933`, (2017).

[23] D. Gang, P. Longhi, M. Romo, and M. Yamazaki, *to appear*.

[24] L. Hollands and A. Neitzke, *Spectral networks and Fenchel-Nielsen coordinates*, Lett. Math. Phys. **106** (2016), no. 6, 811–877.

[25] M. Gabella, *BPS spectra from BPS graphs*, `arXiv:1710.08449`.

[26] M. Alim, S. Cecotti, C. Cordova, S. Espahbodi, A. Rastogi, and C. Vafa, *BPS quivers and spectra of complete $N = 2$ quantum field theories*, Commun. Math. Phys. **323** (2013), 1185–1227.

[27] M. Alim, S. Cecotti, C. Cordova, S. Espahbodi, A. Rastogi, and C. Vafa, *$\mathcal{N} = 2$ quantum field theories and their BPS quivers*, Adv. Theor. Math. Phys. **18** (2014), no. 1, 27–127.

[28] S. Fomin and A. Zelevinsky, *Cluster algebras I: Foundations*, J. Amer. Math. Soc. **15** (2002), no. 2, 497–529.

[29] S. Fomin and A. Zelevinsky, *Cluster algebras. IV. Coefficients*, Compos. Math. **143** (2007), no. 1, 112–164.

[30] K. Nagao, Y. Terashima, and M. Yamazaki, *Hyperbolic 3-manifolds and cluster algebras*, to appear in Nagoya J. Math. `arXiv:1112.3106`.

[31] Y. Terashima and M. Yamazaki, *Semiclassical analysis of the 3d/3d relation*, Phys. Rev. **D88** (2013), no. 2, 026011.

[32] T. Kitayama and Y. Terashima, *Torsion functions on moduli spaces in view of the cluster algebra*, Geom. Dedicata **175** (2015), 125–143.

[33] A. B. Goncharov, *Ideal webs, moduli spaces of local systems, and 3d Calabi-Yau categories*, `arXiv:1607.05228`, (2016).

[34] D. Xie, *Network, cluster coordinates and $N = 2$ theory I*, `arXiv:1203.4573`.

[35] M. Cirafici, *Line defects and (framed) BPS quivers*, JHEP **11** (2013), 141.

[36] M. Cirafici and M. Del Zotto, *Discrete integrable systems, supersymmetric quantum mechanics, and framed BPS states - I*, `arXiv:1703.04786`.

[37] A. Neitzke and F. Yan, *Line defect Schur indices, Verlinde algebras and $U(1)_r$ fixed points*, `arXiv:1708.05323`.

[38] I. Coman, M. Gabella, and J. Teschner, *Line operators in theories of class $\mathcal{S}$, quantized moduli space of flat connections, and Toda field theory*, JHEP **10** (2015), 143.

[39] G. W. Moore, A. B. Royston, and D. Van den Bleeken, *Parameter counting for singular monopoles on $\mathbb{R}^3$*, JHEP **10** (2014), 142.

[40] G. W. Moore, A. B. Royston, and D. Van den Bleeken, *Brane bending and monopole moduli*, JHEP **10** (2014), 157.

[41] G. W. Moore, A. B. Royston, and D. Van den Bleeken, *Semiclassical framed BPS states*, JHEP **07** (2016), 071.

[42] G. W. Moore, A. B. Royston, and D. Van den Bleeken, *L^2-kernels of dirac-type operators on monopole moduli spaces*, `arXiv:1512.08923`.

[43] T. D. Brennan and G. W. Moore, *A note on the semiclassical formulation of BPS states in four-dimensional $N = 2$ theories*, PTEP **2016** (2016), no. 12, 12C110.

[44] T. Dimofte and S. Gukov, *Chern-Simons theory and S-duality*, JHEP **05** (2013), 109.

[45] D. Gang, E. Koh, S. Lee, and J. Park, *Superconformal index and 3d-3d correspondence for mapping cylinder/torus*, JHEP **01** (2014), 063.

[46] D. Gaiotto, G. W. Moore, and A. Neitzke, *Wall-crossing, Hitchin systems, and the WKB approximation*, Adv. Math. **234** (2013), 239–403.

CENTER FOR THEORETICAL PHYSICS
SEOUL NATIONAL UNIVERSITY, SEOUL 08826, KOREA
E-mail address: `arima275@snu.ac.kr`

DEPARTMENT OF PHYSICS AND ASTRONOMY
UPPSALA UNIVERSITY, BOX 516, SE-75120 UPPSALA, SWEDEN
E-mail address: `pietro.longhi@physics.uu.se`

KAVLI INSTITUTE FOR THE PHYSICS AND MATHEMATICS OF THE UNIVERSE
(WPI), UNIVERSITY OF TOKYO, CHIBA 277-8583, JAPAN
E-mail address: `masahito.yamazaki@ipmu.jp`